Stockholm University

Master Thesis

Degree Project in Marine Geology 60 hp

Wetland development and paleoclimate reconstruction based on two Late Holocene sequences from Sani Valley, Lesotho highlands, Drakensberg

Caroline Bringensparr

Stockholm 2016

Department of Geological Sciences
Stockholm University
SE-106 91 Stockholm
Sweden

SAMMANFATTNING

Våtmarksutveckling och paleoklimatrekonstruktion baserat på två sen-Holocena sekvenser från Sanidalen, Lesotho, Drakensberg

Studien av våtmarker ur ett paleoklimatologiskt perspektiv har ökat de senaste åren, på grund av deras potential att bevara klimatsignaler och dess inflytande på förståelsen av kortvariga klimatförändringar. Här har olika kemiska och fysiska analyser använts för att fastställa förändringar i mängden mineralmaterial (Si/Ti, Zr/Ti, bulk density), redox-förhållanden (Fe/Ti, Mn/Ti) och biologisk produktivitet (Ca/Ti, C/N, diatoméer) för två våtmarker i Lesotho: Ladybird (LB) och Frog Springs (FS). Fyra enheter med liknande karaktär har identifierats för båda siterna och representerar utvecklingen av dessa våtmarker sedan starten av den organiska ackumulationen vid ca. 2 800 cal yr BP (FS) och 1 300 cal yr BP (LB). Den föreslagna utvecklingsvägen är att fördjupningar skapade från vind- och vattenerosion har agerat grund för bildningen av mindre dammar som senare har fyllts igen med minerogent och organiskt material. Med tiden har detta övergått till ett stadie där våtmarken är fullt utvecklad, som idag. Denna utveckling har länkats till andra studier i Lesotho samt andra delar av södra Afrika.

ABSTRACT

Wetland development and paleoclimate reconstruction based on two Late Holocene sequences from Sani Valley, Lesotho highlands, Drakensberg

The study of wetlands in a paleoclimatological context has increased in the last years, because of its potential to preserve climate signals and as the understanding of its importance in short term climate change has grown. Here, several chemical and physical proxies have been used to determine changes in detrital input (Si/Ti, Zr/Ti, bulkdensitet), redox conditions (Fe/Ti, Mn/Ti) and biological productivity (Ca/Ti, C/N, diatoms) at two wetland sites in Lesotho: Ladybird (LB) and Frog Springs (FS). Four units of similar character have been identified at both sites and represent the development of these wetlands since the initiation of organic accumulation around 2 800 cal yr BP (FS) and 1 300 cal yr BP (LB). The proposed development path is that alpine pans, formed from aeolian and fluvial erosion, have been the basis for the development of ponds and puddles that have later been infilled with mineral and organic matter, which in time have led to the transition into a wetland stage, as there is today. This development has been linked to other studies in Lesotho and other parts of southern Africa.

Contents

1. INTRODUCTION 5

1.1. PROJECT AIMS 6

2. SETTING 7

3. BACKGROUND 10

3.1. WETLANDS AND ORGANIC DEPOSITS 10

3.2. CLIMATE 12

4. MATERIAL AND METHODS 14

4.1. FIELD WORK 14

4.2. SAMPLE PREPARATIONS 14

4.3. BULK DENSITY 14

4.4. RADIOCARBON DATING 15

4.5. X-RAY FLUORESCENCE (XRF) METHODS 15

4.5.1. SCANNING XRF 15

4.5.2. WD-XRF 15

4.6. DIATOMS 15

4.7. C/N ANALYSIS 15

4.8. LOI – LOSS ON IGNITION 16

4.9. PCA – PRINCIPAL COMPONENT ANALYSIS 16

5. RESULTS 17

5.1. LB 17

5.1.1. CHRONOLOGY 17

5.1.2. STRATIGRAPHY 18

5.1.3. BULK DENSITY 18

5.1.4. ASH CONTENT 19

5.1.5. CARBON AND NITROGEN CONTENT 19

5.1.6. ELEMENTAL VARIATIONS 20

5.2. FS 23

5.2.1. CHRONOLOGY 23

5.2.2. STRATIGRAPHY 24

5.2.3. BULK DENSITY 24

5.2.4. ASH CONTENT 25

5.2.5. CARBON AND NITROGEN CONTENT 25

5.2.6. ELEMENTAL VARIATIONS 26

6. DISCUSSION 29
6.1. ELEMENTAL VARIATION CONTROLS 30
6.2. DETRITAL INPUT CONTROLS 31
6.3. ORGANIC MATERIAL CHARACTERIZATION 33
6.4. LB UNITS 34
Unit D (109-86 cm) 34
Unit C (86-65 cm) 35
Unit B (65-15 cm) 35
Unit A (15-0 cm) 35
6.5. FS UNITS 36
Unit C (144-118 cm) 36
Unit X (118-91 cm) 36
Unit B (91-66 cm) 36
Unit A (66-0 cm) 37
6.6. WETLAND DEVELOPMENT 37
6.6.1. CHRONOLOGY & AGE REVERSALS 40
6.7. COMPARISON WITH OTHER STUDIES AND FUTURE RESEARCH 41
7. CONCLUSIONS 43
8. ACKNOWLEDGEMENTS 44
REFERENCES 45
APPENDIX A – METHOD DESCRIPTIONS 50
CALCULATING SAMPLE AREAS IN INKSCAPE 50
ENRICHMENT AND MOUNTING OF DIATOMS 50
APPENDIX B – XRF CORRELATION MATRICES 52
INTERELEMENTAL CORRELATION MATRICES 52
XRF CORRELATIONS 54

List of Figures

FIGURE 1 LOCATION OF THE TWO SAMPLE LOCATIONS 7

FIGURE 2 LOCATION OF SANI PASS IN LESOTHO 8

FIGURE 3 LB SITE FROM THE SOUTHERN HILLSIDE 9

FIGURE 4 FS SITE FROM UPSTREAM 9

FIGURE 5 THÚFUR, SOIL MOUNDS 11

FIGURE 6 RAINFALL ZONES IN SOUTHERN AFRICA 12

FIGURE 7 AGE-DEPTH MODEL FOR LB 17

FIGURE 8 RADIOGRAPH OF CORE B1-C1 FROM LB 18

FIGURE 9 LB, RESULTS FROM C/N ANALYSIS 19

FIGURE 10 SCANNING XRF ELEMENTAL VARIATIONS, LB 21

FIGURE 11 LB, TI-RATIOS 22

FIGURE 12 AGE-DEPTH MODEL FOR FS 23

FIGURE 13 RADIO-GRAPH OF CORE FS C1 24

FIGURE 14 FS, RESULTS FROM C/N ANALYSIS 25

FIGURE 15 SCANNING XRF ELEMENTAL VARIATIONS, FS 27

FIGURE 16 TI-RATIOS 28

FIGURE 17 RADIOGRAPH OF CORE B2-C2 FROM LB 35

FIGURE 18 AERIAL PHOTOGRAPH OF THE SANI VALLEY 39

FIGURE 19 AERIAL PHOTOGRAPH OF THE SANI VALLEY 39

FIGURE 20 SCHEMATIC OVER WETLAND DEVELOPMENT 40

1. Introduction

The study of wetlands in a paleoclimatological context is important as it provides a unique insight into past environments and can help understand ongoing and future climate changes. The wetlands of Lesotho are the main water reserve in southern Africa (Grab, 2010), and are today subject to anthropogenic damage in the form of drainage, cattle crazing, mining and pollution (Grundling et al., 2014), in addition to the natural variations that occur following a changing climate. It is therefore important to distinguish natural variations from anthropogenic effects, so that actions can be taken in order to preserve these very important water reserves for future generations. Unfortunately, the understanding of the late Holocene climate history of these wetland areas is poor and is based mainly on finds from archaeological studies (Parker et al., 2011). This study is one step closer to comprehending past and recent processes acting in these areas, and provides an insight into climate and wetland changes over the last 2 800 years.

Minerotrophic wetland environments are mainly fed by groundwater, with additional water input from precipitation and surface runoff (Charman, 2002). This means that the geochemical characteristics differs from a mainly atmospherically fed wetland (ombrotrophic), as the composition of the bedrock needs to be considered, as well as the effect groundwater penetration might have on the geochemistry of the sediments. Changes in temperature, and more importantly precipitation, are key factors to changes in the environment where wetlands can form and develop (Kylander et al., 2013a). These affect both the rate at which wetland vegetation can grow, as well as to what extent buried material can be decomposed.

Paleoclimatological reconstructions of wetlands, are most common in the northern hemisphere, especially in northern Europe (Chambers et al., 2012). Research have also been conducted in several locations in North America (Chambers et al., 2010) and China (Hong et al., 2001; Large et al., 2009), but there have also been several studies focusing on wetlands in the southern hemisphere, e.g. Australia (Kylander et al., 2007; Muller et al., 2008), Easter Island (Margalef et al., 2013), Borneo (Weiss et al., 2002) and southern Africa (Norström et al., 2014). The wetlands of Lesotho have been studied in paleoclimatic and environmental contexts earlier (e.g. Backéus 1989; Grundling et al., 2014; Olaleye et al., 2014; van Zinderen-Bakker & Berger 1974), but to my knowledge, this is the first multi-proxy paleoclimate study based on organic-rich sediments from spring fed wetlands in the area.

Here, the results from several exploratory organic sequences from the Sani Valley are presented and interpreted in order to understand wetland development and evidence of climate changes during the last ca. 2800 years. The organic-rich sediments have been analyzed for a series of chemical and physical proxies, e.g. elemental variations, bulk density, ash content and carbon isotope variations. These proxies can alone, and together, aid in the interpretation of mineral matter origin, characterization of organic material and finally in reconstructing the hydrological changes that have taken place during the time period covered by the sequences.

1.1. Project aims

This study has focused on investigating how different chemical and physical proxies can be used to unravel the history of the accumulation environment for organic-rich sediment from two high-altitude sites in Lesotho. The main objectives and the aims of the project have been to:

- Identify the main controls on the mineral material in the deposit, based on chemical and physical proxies
- Characterize the composition of the organic material
- Characterize the geomorphology and hydrology of the basins where these deposits are found
- Reconstruct changes in fluvial, atmospheric and possibly volcanic activities, during the time span covered by the sequences and investigate whether these can be related to established climate changes in southern Africa.

2. Setting

The Sani Valley is situated in the uKhahlamba (Drakensberg) range of the Maluti Mountains, near the Great Escapment, which acts as a natural divider between the KwaZulu-Natal province of South Africa and the Thaba-Tseka region of Lesotho (Grundling et al., 2014; Knight & Grab, 2015). This part of Lesotho is home to the highest peaks in Africa, south of Mount Kilimanjaro, with Thabana Ntlenyana being the highest at 3 482 m a.s.l. (Nel & Sumner, 2008). Along Sani Pass, the road leading up to Lesotho, the upmost bedrock layer consists of Jurassic amygdaloidal tholeiitic basalt of the 625 m thick Lesotho unit (Ramluckan, 1992). Below there are another 175 m of basalt before reaching the white sedimentary bedrock of the Karoo Supergroup (Mitchell & Ramluckan, 1996). The vegetation in the high-altitude parts of Lesotho (ca 2 300-2 900 m a.s.l.) consists mainly of grasslands, with the species *Themeda triandra* and *Festuca caprina* dominating, while the alpine zone (>2900 m a.s.l.) are dominated by heath such as *Erica dominans* and *Passerina montana* (Grundling et al., 2014). On and near wetland areas, different types of herbs and sedges are the dominant vegetation, e.g. *Isolepis angelica, Cotula pludosa, Athrixia fontana* and *Haplocarpha nervosa* (Grab, 2012).

The two wetland sites studied here are Ladybird (LB) at 2 890 m a.s.l. and Frog springs (FS) at 2 835 m a.s.l., located approximately 2.5 km apart (Figure 2). The area is grazed mainly by sheep and is disturbed by the activity of the local burrowing rodents, ice-rats. Although sampling occurred during a dry period (May) the water table was high enough for the deposits to be wet. Thúfur, soil mounds created from frost heaving, are encountered at both sites, apart from in the very middle of the deposits, where there appears to be a constant flow of spring water suggesting that the water may not freeze, even during winter.

Figure 1 Location of the two sample locations, Frog Springs (2 835 m a.s.l.) and Ladybird (2 890 m a.s.l.), near the border between Lesotho and South Africa. They are located approximately 2.5 km apart. Source: satellite image from Google Earth.

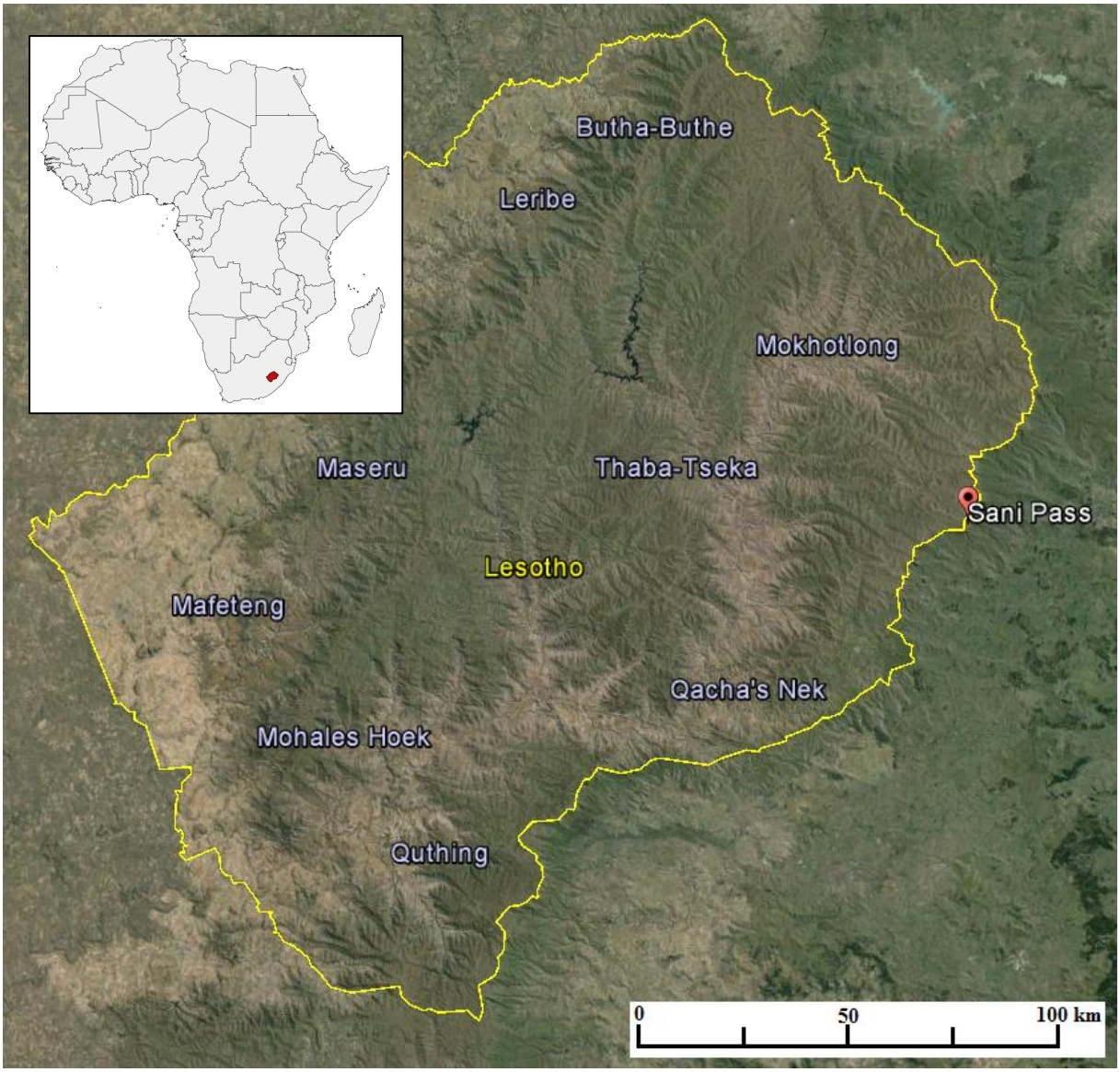

Figure 2 Location of Sani Pass in Lesotho, inset map shows location of Lesotho in Africa (red). Sources: Satellite image from Google Earth, inset map created in QGIS, from vector files downloaded from http://thematicmapping.org/downloads/world_borders.php.

LB site (Figure 3) is located closest to the Great Escarpment and is situated between medium-steep hillsides covered with low shrub-like plants and low grasses. In certain places along the hillsides there is very little or no soil or vegetation, with the bare bedrock exposed. In the middle of this deposit there is a spring pouring out groundwater, which have caused the middle of the site to be slightly elevated. A couple of meters downhill from the spring, there is a shallow pond (ca. 50 cm deep and approximately 1-2 meters in diameter) with standing water. Directly above the pond and the spring outlet, several thúfur can be seen. Approximately 50 meters from the spring mound the ground is quite dry and there are several occurrences of alpine turf exfoliation pans, which are depressions where soil have been removed by wind and/or water (Grab, 2010).

FS (Figure 4) is found ca. 2.5 km north-west of LB, in a rather flat field, and is also situated above a spring, although this site presents a less elevated mound in the middle and have no ponds of standing water. Instead there is numerous thúfur near the spring outlet and within a diameter of 5-10 meters from it, in higher numbers uphill from the spring. Here there is also evidence of catchment runoff water flowing towards the site, in the form of a, at the time for the field work, dried out shallow gully.

Figure 3 LB site seen from the southern hillside, car for scale. Samples taken approximately 10 meters to the left from the car, above the spring mound in the center of this basin. In the foreground, the low vegetation growing on the hillsides.

Figure 4 FS site seen from upstream, car for scale. In the foreground of the image, a gully created from catchment runoff can be seen in between patches of the same low vegetation as that found at LB site.

3. Background

3.1. Wetlands and organic deposits

Generally speaking, wetlands can be divided into two types: atmospherically fed ombrotrophic wetlands and minerotrophic wetlands, receiving their water from groundwater, run-off and precipitation (Charman, 2002). Wetlands are essentially deposits of organic material, and they are formed when the production of organic matter exceeds the rate of decomposition. In addition to this, certain water conditions need to be met i.e. a high enough water table for the wetland to be water-logged during the better part of a year (e.g. Charman, 2002; Meadows, 1988). This water-logging, in combination with cool climate, enables a better preservation of organic material, instead of it being decomposed. In wetlands, the aerobic decay of plants, resulting in carbon loss, takes place in the acrotelm (top layers), while anaerobic decay take place in the catotelm (below the water table), releasing methane (CH_4) (Chambers et al., 2010). The main driving forces for organic matter growth is temperature and precipitation, why accumulation during summer conditions dominate (Kylander et al., 2013a). Minerotrophic wetland deposit are, as the name suggests, consisting of a varying fraction of the minerogenic material, which is brought to the site from the catchment with surface runoff or by winds from longer distances.

The wetlands of the high-altitude areas of Lesotho act as the principal water reserve in southern Africa (Grab 2010) and have earlier been studied to some extent by e.g. Zinderen Bakker & Werger, (1974), Olaleye et al. (2014) and Backéus & Grab (1995). A compilation of studies published up to 2002 are presented in the IMPESA report (Sliva & Grundling, 2002), where it was estimated that the wetlands in Lesotho have a combined area of about 18-20 km^2. Wetlands can be found in all parts of the country, although very sparsely distributed in the lowlands (1400-1800 m a.s.l) (Backéus & Grab, 1995). In the high-alpine areas (>2750 m a.s.l.) they are usually found in flat areas, in north facing concave slopes or adjacent to watercourses such as the Orange River and the Sani River (Grundling et al 2014). Their classification has varied, from the most common mires (Grundling et al., 2014; Backéus & Grab, 1995), to fens (Sliva & Grundling, 2002) and bogs (van Zinderen Bakker & Werger, 1974), but as the wetlands studied here do not fit any of the widely accepted definitions, they will hereafter simply be referred to as minerotrophic wetlands.

The wetland sites of the Sani Valley are mainly groundwater fed, in addition to receiving water from precipitation and surface runoff from the surroundings (Backéus, 1989, Backéus & Grab, 1995). This type of spring fed wetlands are not very common, but can be found in southern Africa as well, e.g. Wonderkrater (McCarthy et al., 2010) and Lesotho (Backéus, 1989). Studies on spring fed wetlands have also been conducted in other parts of the world, e.g. in East Africa (Ashley et al., 2002), Tasmania (Macphail et al., 2001) and Poland (Dobrowolski et al., 2012; Mazurek et al., 2014).

As the climate of Lesotho is rather cold all year round, this results in slower growth and hence the accumulation rate of organic material (peat) is rather low, around 0.25 mm/yr (Grundling et al., 2014). Previous studies have also shown that the organic accumulation is occasionally interrupted, likely because of increased inwash from eroded slopes in the surroundings, which have been encountered in the form of gravel layers intruding the organic deposits (Marker, 1994; 1995). The cold climate also results in thúfúr (Figure 5), mounds caused by frost heaving, which are common occurrences on or adjacent to the wetlands in the high-alpine zone, and are about 15 cm high and 50-70 cm in diameter (Backéus & Grab, 1995; van Zinderen Bakker & Werger, 1974).

Figure 5 Thúfur, soil mounds created from repeated frost action causing the soil to expand. Photo from LB.

3.2. **Climate**

Southern Africa lies at the intersection of three oceans and several climate systems, of which the intertropical convergence zone (ITCZ), the westerlies and Southern Ocean frontal systems are the most important (Chase & Meadows, 2007: Mills et al., 2012). Three rainfall zones have been defined for southern Africa: the summer rainfall zone (SRZ) to the north-east, the winter rainfall zone (WRZ) along the coasts to the south and west and the year round rainfall zone (YRZ) as a narrow region between the other two (Figure 6) (Chase & Meadows, 2007). The part of Lesotho studied here falls within the SRZ.

The present day climate of Lesotho seems to be a subject of discussion, although rather reliable temperature and precipitation data exists (e.g. Nel & Sumner, 2008: Sene et al., 1998). The climate has been defined differently by different authors, and the definitions varies from "alpine and seasonal" (van Zinderen Bakker & Werger, 1974), "temperate and continental" (Olaleyle et al., 2014), "semiarid to subhumid and continental, temperate" (Schmitz & Rooyani, 1987) to "marginal periglacial" (Nel & Sumner, 2008). Taking all these into account a more fitting definition of the climate in this region might be "alpine temperate", as was also suggested by Backéus & Grab (1995).

Annual mean air temperatures have been estimated to around 6 ºC at high altitudes (above 2500 m a.s.l.) (Grab, 1997; Nel & Sumner, 2008), with summer temperatures reaching up to 16 ºC. The winter months (June to August) are dry and cold and reach mean temperatures of

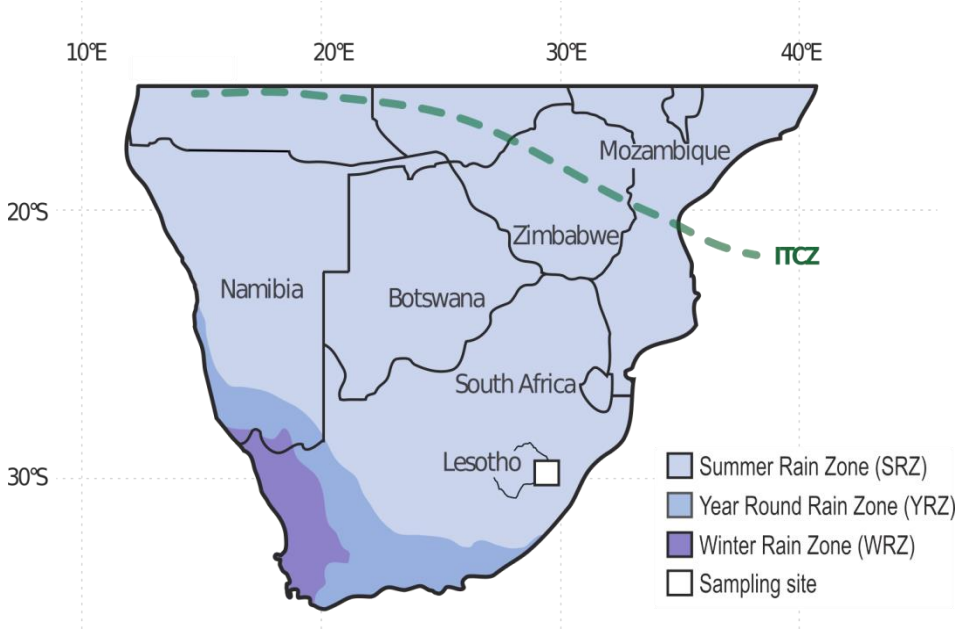

Figure 6 Schematic illustration of the rainfall zones in southern Africa, see legend. Lesotho is situated within the Summer Rain Zone (WRZ). The Intertropical Convergence Zone (ITCZ) is marked with a green dotted line.

approximately 0 ºC (Grab 2002), occasional snowfall events (Grundling et al., 2014; Backéus & Grab, 1995) and strong northwesterly winds (Grab 2010). In a study made by Grab (2010) in 2001, wind speeds up to 26.75 m/s were measured in April with maximum wind gusts of over 30 m/s, and the period with strongest mean wind speeds is in late winter/spring (August-October).

There have also been discussions about the mean annual precipitation, based on measurements made with rain gauges placed at certain locations in Lesotho. Especially interesting for this study are those placed near the escarpment edge in the vicinity of Sani Top. These values have been extrapolated to cover longer time frames and have presented mean annual precipitation values ranging from ca. 800 to 1600 mm (Grab, 2010; Sene et al., 1998). Nel & Sumner (2008) measured a mean annual precipitation of 767.8 mm at Sani Pass over the course of 4 years (2001-2005) and mentions that paleoprecipitation estimates based on extrapolation of existing precipitation measurements, should be made with caution for values higher than 1000 mm per year. However, they also state that the period during which precipitation measurements were made was dryer than the long-term averages. The areas of Lesotho receiving most precipitation lies to the east, near the escarpment edge, with decreasing precipitation rates inland to the west, where most of the interior uplands are in rain shadow (Grundling et al., 2014; Parker et al., 2011). Most of the summer precipitation falling in eastern Lesotho has its origin in moisture transported from the Indian Ocean (Chase et al., 2015), forming orographic precipitation upon reaching the steep walls of the eastern Drakensberg range (Sene et al., 1998).

4. Material and methods

4.1. Field work

The samples were collected from a wetland area in the Sani Valley, Lesotho, southern Africa in May 2015. The cores were retrieved using a Russian corer with a plastic liner length of 50 cm and an inner diameter of 4.75 cm. A preliminary stratigraphic description was made in the field immediately after core retrieval, before being covered in plastic film to prevent dehydration, contamination and mold growth. After transport to Sweden, all cores were stored at IGV in a cold room at 4 ºC, until they were sub-sampled.

Two sites were sampled, resulting in the retrieval of a total of thirteen cores, six of which have been analyzed in this project. From LB five overlapping cores were retrieved from two boreholes, circa 10 cm apart. (Borehole 1: B1-C1: 0-50, B1-C2: 50-100 cm, B1-C3: 65-115 cm; Borehole 2: B2-C1: 25-75 cm, B2-C2: 65-115 cm). From FS three consecutive cores were retrieved from one borehole (C1: 0-50 cm, C2: 50-100 cm, C3: 95-145 cm). Two additional cores were retrieved from a site adjacent to FS, but were later discarded due to their low organic and high coarse minerogenic content. All analyses, unless otherwise stated, were performed at the Department of Geological Sciences, Stockholm University.

4.2. Sample preparations

The cores were sub-sampled using a stainless steel knife, at 1 cm intervals. About one quarter of each sample was saved in plastic bags in a cold room for diatom analysis, and the remainder of the samples were freeze-dried at –59 °C in a Scanvac CoolSafe 55-4 Pro for three days. Selected samples were milled for 2 minutes at 30 strokes per second in a Lab Wizz Type 320 Micro Ball Mill.

4.3. Bulk density

Dry bulk densities [g/cm^3] of the samples were based on dry mass (m) of the samples after freeze-drying, thickness (L) measured with calipers and sample areas (A) measured digitally using Inkscape, see Appendix A-1. The dry bulk density (ρ) was calculated as:

$$\rho_{bulk} = \frac{m_{dry}}{A_{sample} L_{sample}}$$

Results from the bulk density calculations were used for a preliminary core alignment, later adjusted based on other data, see below.

4.4. Radiocarbon dating

Macrofossils (plant parts) were picked under a microscope and sent to Beta Analytic Radiocarbon Dating laboratory in London for Accelerator Mass Spectrometry (AMS) dating. A total of 11 samples between 40.60 and 103.5 cm (adjusted depth) in the LB sequence and between 30.50 and 128.9 cm (adjusted depth) in the FS sequence were dated.

4.5. X-ray fluorescence (XRF) methods

4.5.1. Scanning XRF

Relative elemental concentrations as well as optical and X-radiographic images of whole cores were attained on a Cox Analytical Systems ITRAX XRF Core Scanner (Gothenburg, Sweden), using a molybdenum (Mo) tube at 200 ms exposure time, 50 kV, 40 mA, and a step size of 200 µm. For technical specifications of the instrument, refer to Croudance et al. (2006). Prior to analysis a couple of millimeters were scraped off of each core with a stainless steel blade to minimize contamination from material that might have relocated during sampling and transport.

4.5.2. WD-XRF

Absolute concentrations were measured on milled bulk samples on a Bruker S8-Tiger WD-XRF (wavelength dispersive x-ray fluorescence) analyzer equipped with a Rh-anticathode X-ray tube, at the Department of Ecology and Environmental Sciences, Umeå University by Johan Rydberg. Based on the aligned cores, samples for analysis were chosen with 5 cm intervals, totaling to 79 samples, with an additional 10 duplicates. Between 490 and 510 mg of each sample were weighed into 20 mm plastic cups, covered at the bottom with a 2 µm thick Mylar plastic film.

4.6. Diatoms

Samples for diatom analysis were taken at approximately every 10 cm from FS2 and preparation was performed at IGV following the procedure described by Battarbee et al. (2001), with a few exceptions (see Appendix A for a detailed preparation schedule). Samples mounted on glass slides were analyzed and interpreted by Dr. Jennifer Fitchett at the University of the Witwatersrand, Johannesburg, South Africa.

4.7. C/N analysis

C/N analysis was made at a 5 cm sample resolution, with a total of 52 samples, 23 from LB and 29 from FS. Between 0.5 and 15 mg sample (weight based on organic content) were weighed into tin cups and analyses was performed in a Finnigan DeltaV advantage flow mass

spectrometer coupled with a CarloErba NC2500 elemental analyzer, by Heike Siegmund. Six samples were acid treated with hydrochloric acid (HCl) prior to analysis to detect any occurrence of carbonates.

4.8. LOI – Loss on ignition

Approximately 0.5-1 g sample was weighed into crucibles that were put in an oven overnight at 105°C and dried to a constant weight. They were then placed in an oven at 450°C overnight, and weighed once cooled to circa 40°C.

4.9. PCA – Principal component analysis

Interelemental correlation matrices based on Z score values (to avoid scaling effects) from the scanning XRF data were created using principal component analysis in JMP v 12.0.1, in correlation mode using a varimax rotation.

5. Results

The maximum retrieval depth of organic material was 115 cm for LB and 145 cm for FS, as it was not possible to penetrate the gravelly layer at the bottom with the Russian corer. The cores were later aligned using the stratigraphy, bulk density, C/N data and the XRF measurements (see below). A total of six cores were chosen and analyzed for this study, rejecting the two cores from the site adjacent to FS due to their low organic content. Out of the five cores retrieved from LB, three were chosen for best overlap, resulting in cores: B1-C1, B2-C1 and B2-C2. All three cores from FS were used.

5.1. LB

The sequence from LB, which is considered continuous, was divided into four units, based on stratigraphy, bulk density and ash content. This division represents the different lithological units, with sharp transitions to the units above and below. The four units are: A (0-15 cm), B (15-65 cm), C (65-86 cm) and D (86-108.85 cm). The upmost 10 cm of LB are not considered here, apart from in the bulk density and ash content, as these layers are likely to have been disturbed in some way. This can be seen in the radiograph (Figure 8), where the upmost ca. 10 cm is displayed in darker color, suggesting more minerogenic material.

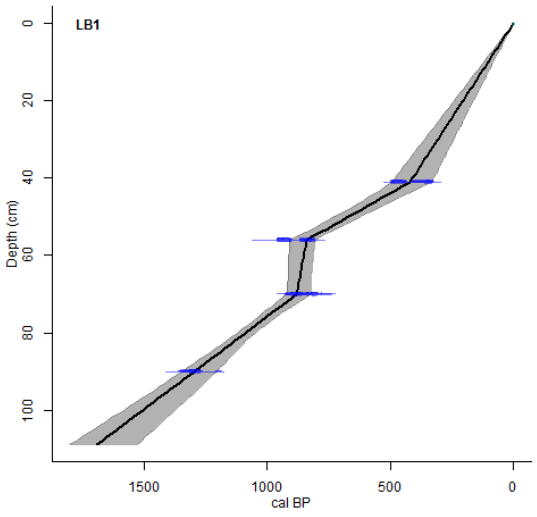

Figure 7 Age-depth model, created using the clam software in R (Blauuw, 2010), for LB. Depth in cm and age in cal yr BP.

5.1.1. Chronology

Five samples from LB were dated with AMS and calibrated using the SHCal13 calibration curve (Hogg et al., 2013) and the age models were obtained using the Clam software (Blauuw, 2010). The best fit was achieved using smooth spline (smooth=0.3). Dates are extrapolated to the bottom of the core using the extrapolation function in the Clam software.

Table 1 AMS dated samples from LB. Ages in calibrated years before present (BP).

#	Sample name	Age (BP)	+/- (BP)	Depth [cm]
1	LB1 B1 0-50 cm 40-41	390	30	40.60
2	LB1 B2 25-75 cm 50-51	1170	30	55.90
3	LB1 B2 25-75 cm 64-65	960	30	69.55
4	LB1 B2 65-115 cm 77-78	920	30	85.5
5	LB1 B2 65-115 cm 95-96	1390	30	103.5

5.1.2. Stratigraphy

At the very bottom of this sequence was the gravelly layer encountered at 115 cm depth (unadjusted), corresponding to ca. 109 cm adjusted depth. From there up to 92 cm is a somewhat sandy blue-gray layer, gradually darkening upwards. There is some occurrences of interbedded orange to brown layers. Above this, up to 90 cm, the color is gradually lighter, containing some smaller gravel and sand. From 90 to 84 cm, the color is a darker grey-brown, but with similar composition as the previous layer. Between 84 and 75 cm there are interbedded laminations of light grey and darker grey-brown, with a pebble at 80 cm. From 75 cm the organic content increases, color turns to more brown and some plant and root parts can be seen. The material gets more fibrous and less decomposed upwards. From 49 to 36 cm there are no visible plant parts, and the color changes from dark grey-brown to lighter brown. At 36 cm plant parts can again be seen, and the material is slightly fibrous, while at 21 cm there is a transition to very fibrous, poorly decomposed dark black brown material with plenty of plant remains.

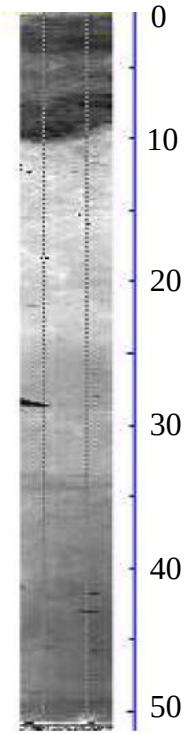

Figure 8 Radiograph of core B1-C1 from LB. Depths in cm. The upper 10 cm displays disturbed sediment.

5.1.3. Bulk density

Out of the 100 samples from LB, poor cohesion led to impaired physical integrity of two samples, which therefore could not be analyzed. Bulk densities varies between 0.27 (17.10 cm) and 1.00 (105.75 cm) g/cm^3 and generally follows a linear decreasing trend ($R^2 = 0,92$) upwards, excluding the top 10 cm. Between 108.85 and 86.25 cm bulk densities oscillate, up to 0.376 g/cm^3 between the highest and lowest value in this sequence. Slight rise at 86.25 to 73.4, with a maximum value of 0.77 g/cm^3. At 69.55 cm there is a peak value of 0.715 g/cm^3. The drop around 50 cm is a core boundary. From 47.1 to 17.1 there is a decrease of 0.32 g/cm^3, after which there is a two-step increase to 0.60 g/cm^3 in the top sample (2.3 cm).

5.1.4. Ash content

The ash content ranges from 52 to 94 %, with highest minerogenic fraction (>95% ash) in the bottommost 40 cm. From the bottom up a slight decreasing trend can be identified, from 94% in the bottom sample (102.65 cm) to about 45 cm, where there is a rapid increase of 7%. Between 20 and 7.20 cm there is a two-step decrease from 69% to 53%, after which values are increasing up to the top layer values of 55%.

5.1.5. Carbon and nitrogen content

Percent carbon varies between 1% (105.75 cm) and 23% (15.10 cm) and follows an increasing linear trend (R^2 = 0.91) up to 15.10 cm, where there is a shift to lower values. $\delta^{13}C$ varies between -28.60‰ (105.75 cm) and -25.95‰ (80.40 cm). $\delta^{13}C$ values increase rapidly from the bottom of the sequence to about 90 cm, where the curve levels out to around -26‰. At 72.5 cm there is a drop to –26.8‰, thereafter a steady decrease up to 13.1 cm (-27.27‰), where the curve again turns towards higher values. The highest C/N ratio values occurs at 105.75 cm (32.83) and has a minimum value of 11.61 at (29.65 cm), with little variation from ca. 63 cm and upwards. From 82.3 cm the C/N ratios increase to a maximum value of 22.59 at 55 cm, after which values decrease back to previous levels around 62.8 cm. Hereafter, there is little variation and the C/N ratio oscillates slightly from a baseline value around 12.

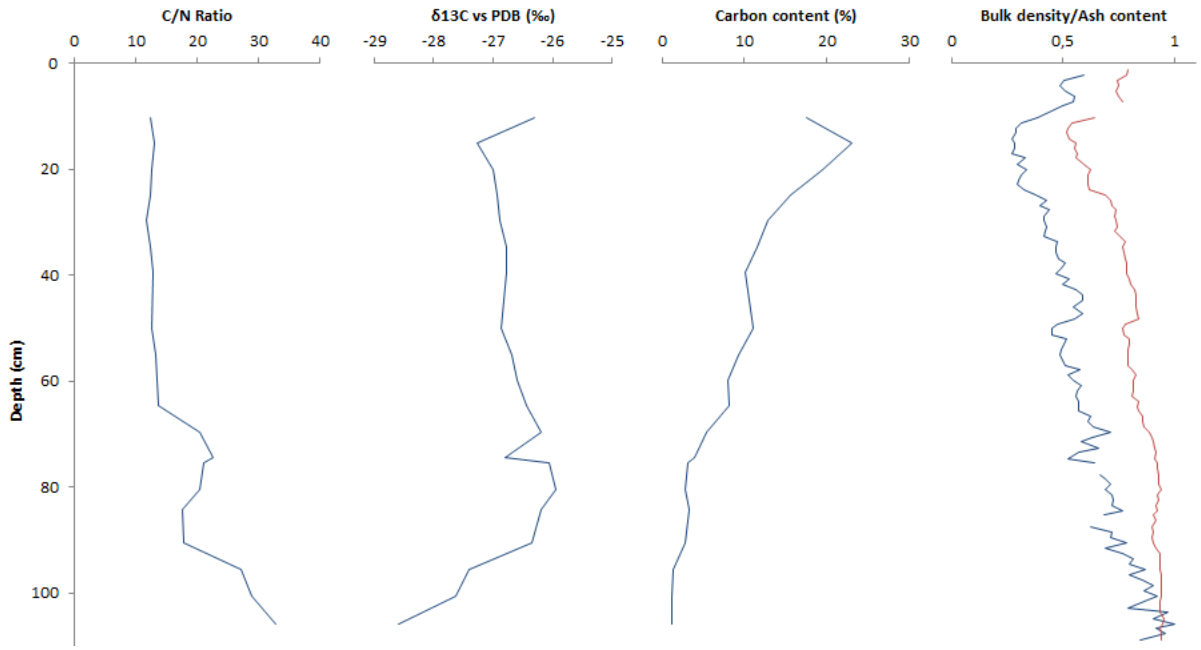

Figure 9 LB, results from C/N analysis: C/N ratio, $\delta^{13}C$ vs. PDB (‰), carbon content (%), bulk density (g/cm^3) and red: ash content (%).

5.1.6. Elemental variations

Si, Ti, Sr and Fe presents generally decreasing trends up to ca. 20 cm, while K, Ca and Mn oscillate from their baseline values throughout the sequence. Above 20 cm, there is a decrease in Si, while Mn, Fe and K increases. The upmost 10 cm are omitted due to core disruption (Figure 8). Around 40 cm there are two drops in Si, Ti, Fe, K and Ca, most likely is due to irregularities in the core surface.

The interelemental correlation matrix for LB (Table 2) presents how different elements correlate to one another. There is coupling between Si and Ti throughout the entire core, with higher amplitude variations in the latter. The general trend is also represented in Fe, K and Ca. Si presents very strong correlation with Ti (>0.86), but also with Ca and K. Over the entire LB sequence Sr correlates well with Ca, Fe, Mn and Ti (>0.79) and K correlates strongly with Ca, Fe, Si, Sr and Ti (>0.81). Zirconium presents strongest correlation with Si and Ti (0.63), and weakest with Mn (0.16). The interelemental correlation does however vary within the units (Appendix B – Table 6).

Table 2 Correlation matrix for standardized ITRAX data from LB. Grey: values under 0.9. Black: Over 0.9 signifies very strong correlation.

	Ca	Fe	K	Mn	Si	Sr	Ti
Fe	0.88						
K	0.94	0.91					
Mn	0.67	0.63	0.58				
Si	0.80	0.63	0.81	0.36			
Sr	0.79	0.87	0.83	0.51	0.53		
Ti	0.90	0.88	0.96	0.50	0.86	0.80	
Zr	0.45	0.40	0.54	0.16	0.63	0.39	0.63

In order to get away from any organic material dilution effects, Ti-ratios for each element were created and are presented in Figure 11. Little variation is seen in Zr/Ti, Mn/Ti and Ca/Ti up to ca. 30-25 cm, with peak values at around 17 cm. Si/Ti presents a generally increasing trend with a drop around 24 cm and peak values at the intersection between unit A and unit B (15 cm). Sr/Ti and Zr/Ti presents peak values at 34, 33 and 29 cm. Mn/Ti and Fe/Ti increases from 20 cm and upwards. Fe/Ti varies little apart from a drop at 90 cm and a peak at 80 cm. Ca/Ti is steadily oscillating up to ca. 70 cm, after which an increasing trend can be seen. Largest peaks can be found at 105, 88 and 15 cm. K/Ti presents a generally increasing trend with peak values at 101, 88 and 15 cm.

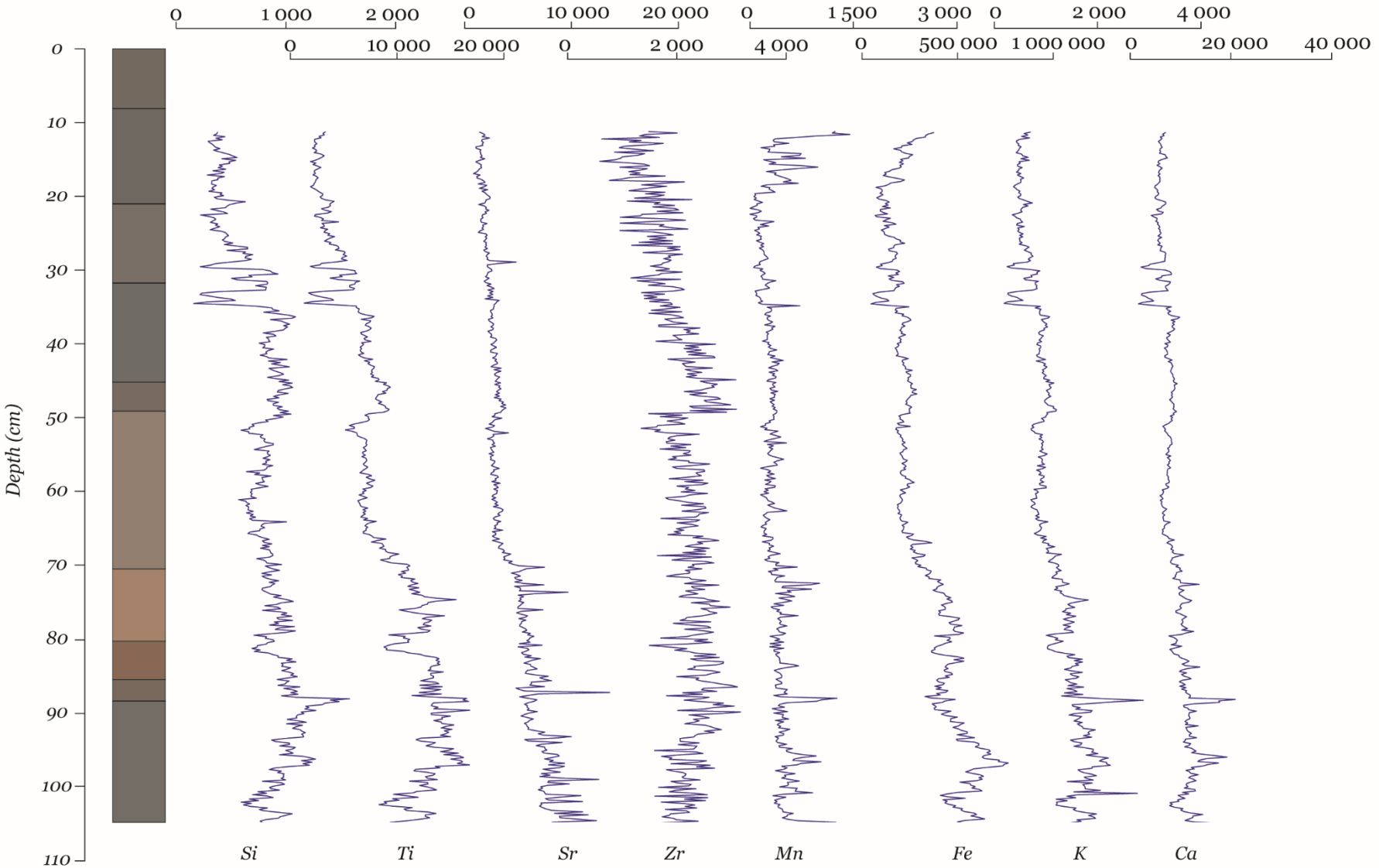

Figure 10 Scanning XRF elemental variations (peak areas) for LB (Si, Ti, Sr, Zr, Mn, Fe, K, Ca). Stratigraphic layers described in the text.

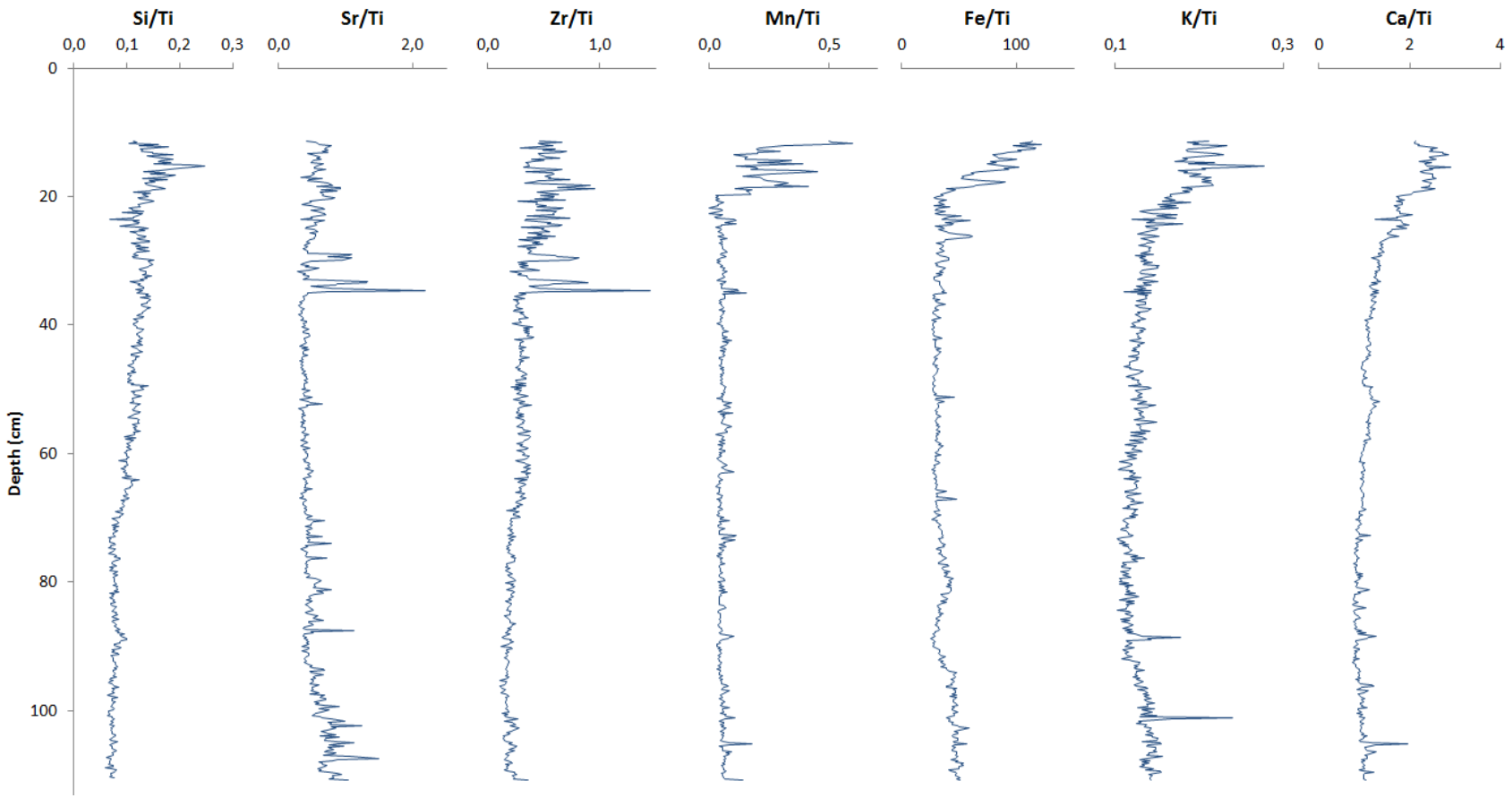

Figure 11 LB, Ti-ratios for elements Si, Sr, Zr, Mn, Fe, K and Ca.

5.2. **FS**

The sequence from FS, considered non-continuous, was divided into four separate units, mainly due to age reversals and X-ray evidence of core disruptions (Figure 13). Boundaries between the units were based on stratigraphy, XRF data and bulk density. It should also be noted that the unit from 91.2 to 118.9 cm have been named X as it presents very different behavior in comparison with the remainder of the data. Reasons for this will be treated in the discussion. The other three units are A (0-65.2 cm), B (65.2-91.2 cm) and C (117.85-143.35 cm).

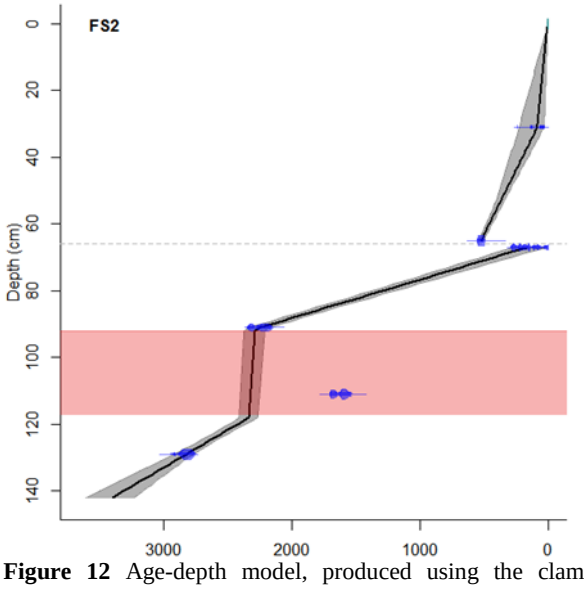

Figure 12 Age-depth model, produced using the clam software in R (Blauuw, 2010), for FS, where date #10 is omitted from the model and the red box represents Unit X. There is a separate age model for the upper ca. 60 cm, due to age reversals between samples #7 and 8

5.2.1. **Chronology**

Six samples from FS were dated using AMS and calibrated using the SHCal13 calibration curve (Hogg et al., 2013). The age models were obtained with Clam software (Blauuw, 2010). The best fit was achieved using smooth spline (smooth=0.3). In the age-depth model for FS, date #10 is omitted from the model and the red box represents Unit X. The upper 65 cm of the sequence presents a separate model because of the age reversals between samples #7 and 8 of ca. 300 years. Dates are extrapolated to the bottom of the core using the extrapolation function in the Clam software.

Table 3 AMS dated samples from FS. Ages in calibrated years before present (BP).

#	Sample name	Age (BP)	+/- (BP)	Depth [cm]
6	FS2 0-50 cm 29-30	20	30	30.50
7	FS2 50-100 cm 64-65	490	30	65.20
8	FS2 50-100 cm 66-67	190	30	67.25
9	FS2 50-100 cm 89-90	2270	30	91.20
10	FS2 95-145 cm 112-113	1700	30	110.75
11	FS2 95-145 cm 130-131	2740	30	128.90

5.2.2. Stratigraphy

At the very bottom of this sequence was the gravelly layer encountered at 145 cm depth (unadjusted), corresponding to ca. 143 cm adjusted depth. From the bottom to ca. 134 cm the color is light grey blue and the composition is sandy clay, with some occurrence of gravel. From 134 to 114 cm, there is a color change to darker grey brown and at 114 cm there is a sharp color change to a light grey layer, with less sand, which continues up to ca. 98 cm. Between 98 and 93 cm there is a more organic layer, dark brown in color, above which is found a layer of alternating blue gray and dark brown laminations up to 85 cm. From 85 cm and upwards there is some visible plant parts, but little variation in the brown grey color. 66 to 51 cm consists of dark brown organic material, with several visible plant parts and roots. 51 to 28 cm consists of decreasing fine-grained minerogenic material and/or decreased decomposition upwards, with gradually lighter brown color and increasing amount of plant parts. At 28 to 26 cm there is a thin layer of lighter brown fibrous material, above which there is a sharp color and composition change to the layer above, which is less fibrous and darker in color. At 21 to 19 cm there is again a thin layer of light brown fibrous material, overlain by the very fibrous top layer, with live vegetation in the top cm.

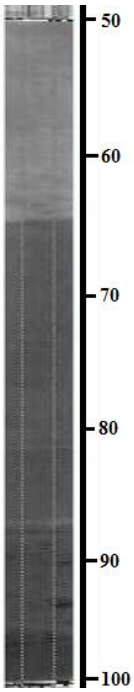

Figure 13 Radiograph of core FS C1. Depth in cm. Disruption at ca. 65 cm.

5.2.3. Bulk density

Bulk density varies between 0.310 (20.35 cm) and 0.919 g/cm^3 (142.35 cm) in the FS2 sequence, with a generally increasing trend downcore. Out of the 141 samples, 13 were too coarse and/or had crumbled and could therefore not be measured. A negative peak can be seen at 133.85 cm (0.65 g/cm^3) after which values decrease up to 114.85 cm (0.54 g/cm^3). Above follows a rise, with a peak of 0.88 g/cm^3 at 109.55 cm, up until 95.30 cm (0.51 g/cm^3). Little variation in densities up to the rapid drop at 66 cm (-0.19 g/cm^3), apart from some oscillations between 0.44 and 0.53 g/cm^3. Above the drop are four distinct peaks at 58.00 (0.47 g/cm^3), 52.05 (0.40 g/cm^3), 48.55 (0.45 g/cm^3) and 30.50 cm (0.50 g/cm^3), after which there is a drop to 0.22 g/cm^3 at 27.30 cm. Around 21-20 cm there is a negative peak (0.13 g/cm^3) and above this the values vary between 0.18 and 0.30 g/cm^3 in the upper 10 cm of the core.

5.2.4. Ash content

The ash contents of FS2 are similar to those of LB1, with values ranging from 46 to 94%. Highest values (>90%) can be found in two intervals of the cores: 105.7-112.75 cm and the bottommost 15 cm. The general trend for the ash content is increasing values downcore, with two larger steps at 25.35 to 30.5 cm (increase of 22% ash) and at 62.25-66.25 cm (increase of 11 %).

5.2.5. Carbon and nitrogen content

Percent carbon varies between 1.29% (143.35 cm) and 30.51% (21.25 cm), with a generally increasing trend upwards, with peaks at 117.85 cm (6.87%), 81.80 cm (10.95%), 61.20 cm (15.30%) and 21.25 cm (30.51%). Above the maximum value, carbon content decreases slightly to the topmost sample at 5.95 cm (5.95%). $\delta^{13}C$ varies between -26.82‰ (16.35 cm) and -25.56‰ (112.75 cm). C/N ratio is highest at 20-21 cm (19.29) and lowest at 30-31 cm (13.84). The general C/N trend is decreasing downcore, with one rise and several peaks at 117.85-97.35 cm (max value: 18.16), 86.85 cm (15.61), 76.55 cm (16.17) and 21.2 cm (19.29).

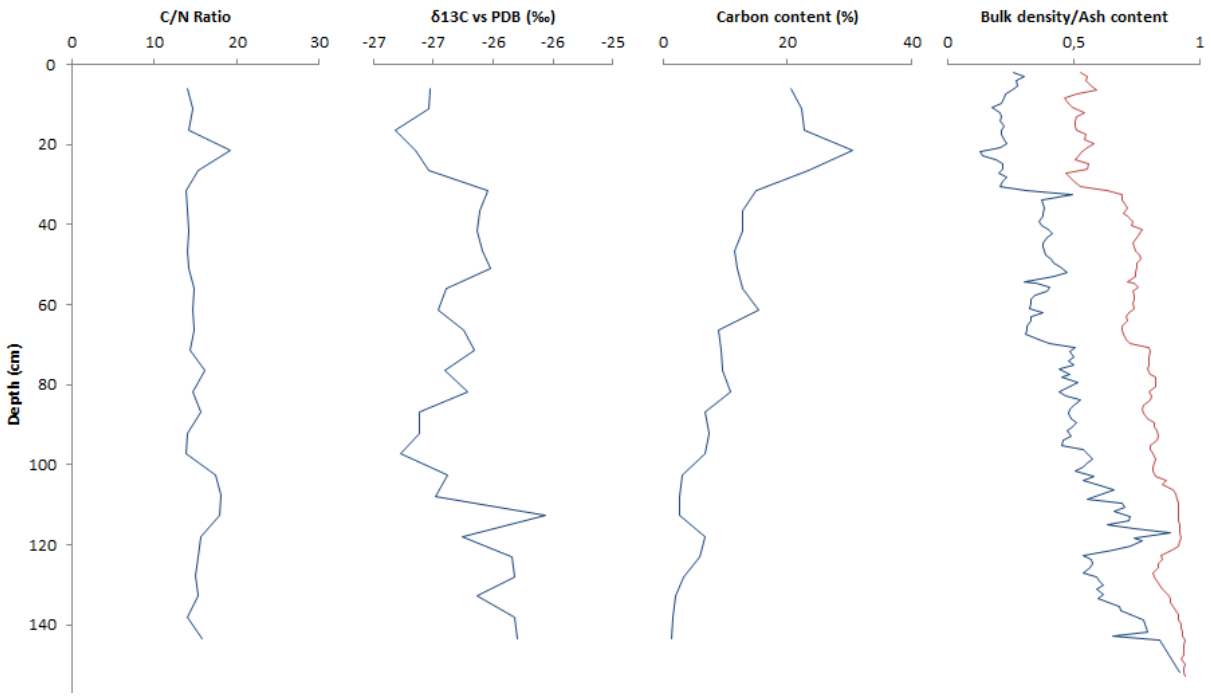

Figure 14 FS, results from C/N analysis: C/N ratio, $\delta^{13}C$ vs. PDB (‰), carbon content (%), bulk density (g/cm^3) and red: ash content (%).

5.2.6. Elemental variations

The elemental variations at FS present a generally decreasing trend for all elements. Part of this trend might however be attributed to differences in core surface elevation, which most likely also is the reason for the abrupt increases at ca. 94 and 50 cm. More variation can be seen at the bottom of the sequence, up to ca. 120 cm, where there is a drop in Ti, Sr, Zr, K and Ca. Strontium presents a peak value at ca. 40 cm. Increase in Ca and Fe can be seen in the upmost 10 cm, which is accompanied by a slight decrease in Sr and Si.

The interelemental correlation matrix for FS (Table 4) presents how different elements correlate to one another. Silica presents strongest correlation with Fe (0.96), while Sr correlates strongest with K and Ti (>0.90). There is generally good correlation between all elements, except for Mn with Fe and Zr. The interelemental correlation does however vary within the different units (Appendix B – Table 7).

Table 4 Correlation matrix for standardized ITRAX data, from FS. Grey: values under 0.9. Black: Over 0.9 signifies very strong correlation.

	Ca	Fe	K	Mn	Si	Sr	Ti
Fe	0.84						
K	0.85	0.94					
Mn	0.48	0.53	0.57				
Si	0.83	0.96	0.94	0.50			
Sr	0.77	0.82	0.92	0.51	0.80		
Ti	0.86	0.95	0.99	0.50	0.95	0.90	
Zr	0.68	0.80	0.88	0.37	0.80	0.86	0.89

In order to get away from any organic material dilution effects, Ti-ratios for each elements were created and are presented in Figure 16. All Ti-rations present a large peak at ca. 10 cm, which most likely is an artifact from changes in core surface. Sr/Ti and Zr/Ti present little variation throughout the sequence, apart from in the top 30 cm, where both increase up to ca. 15, after which they fall back to baseline values. Si/Ti presents a generally increasing trend, with oscillations around a slightly increasing baseline value. Drops can be seen at ca. 90, 80, (50), 35 and 21 cm. Mn/Ti increases 40 fold up to ca. 138 cm, after which it returns to oscillate around baseline values. Fe/Ti decreases slightly up to 120 cm, where there is a sharp increase after which there are high-amplitude oscillations up to the drop at 93 cm. Values then return to the baseline oscillations up to the drop at 50 cm, which is a core boundary. Largest variations can be seen for K/Ti and Ca/Ti, of which the former presents increasing oscillations from baseline values upwards, and the latter presents a generally increasing trend upwards. Ca/Ti peaks at (50), 26, 21, 9 cm.

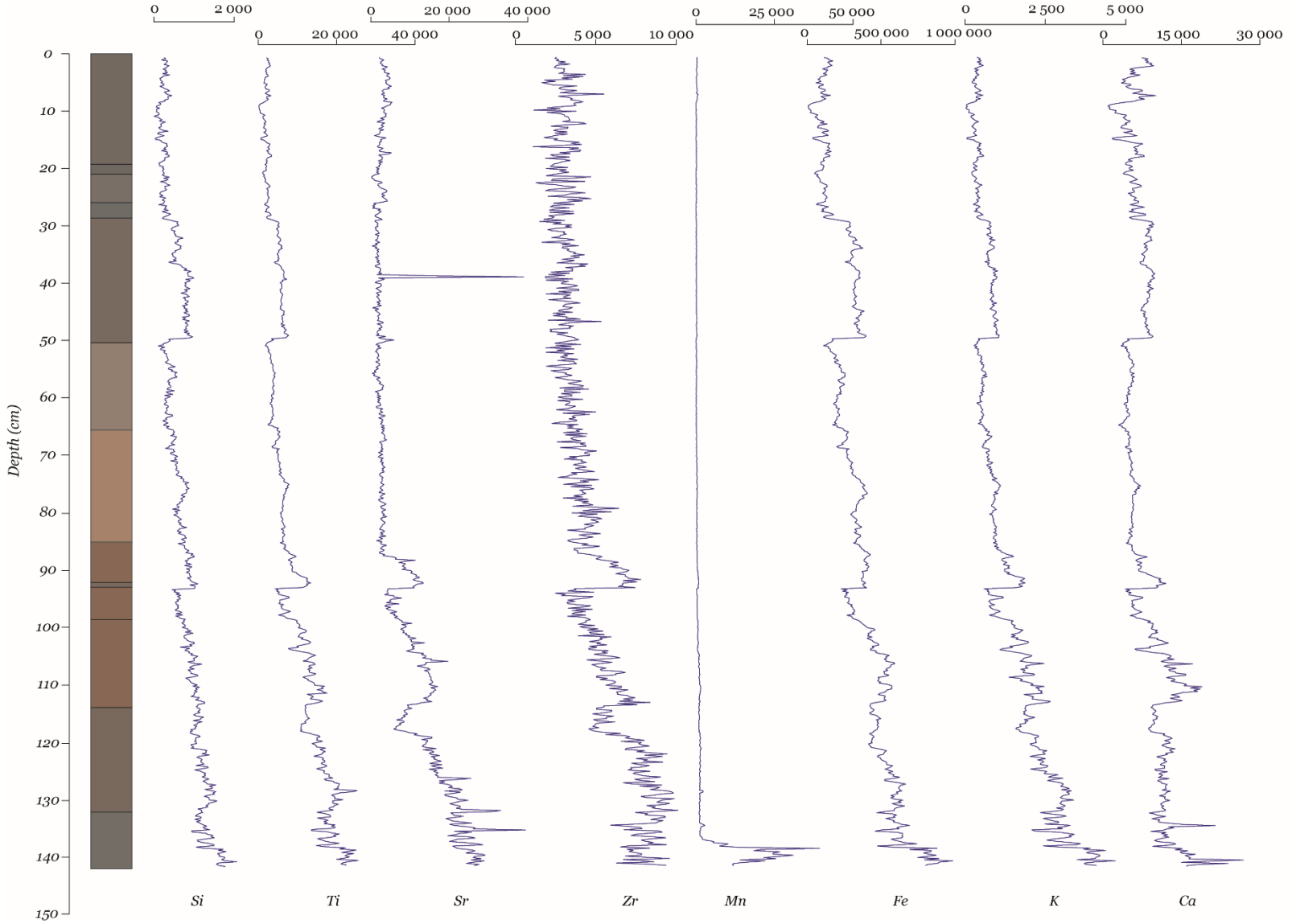

Figure 15 Scanning XRF elemental variations (peak areas) for FS (Si, Ti, Sr, Zr, Mn, Fe, K, Ca). Stratigraphic layers described in the text.

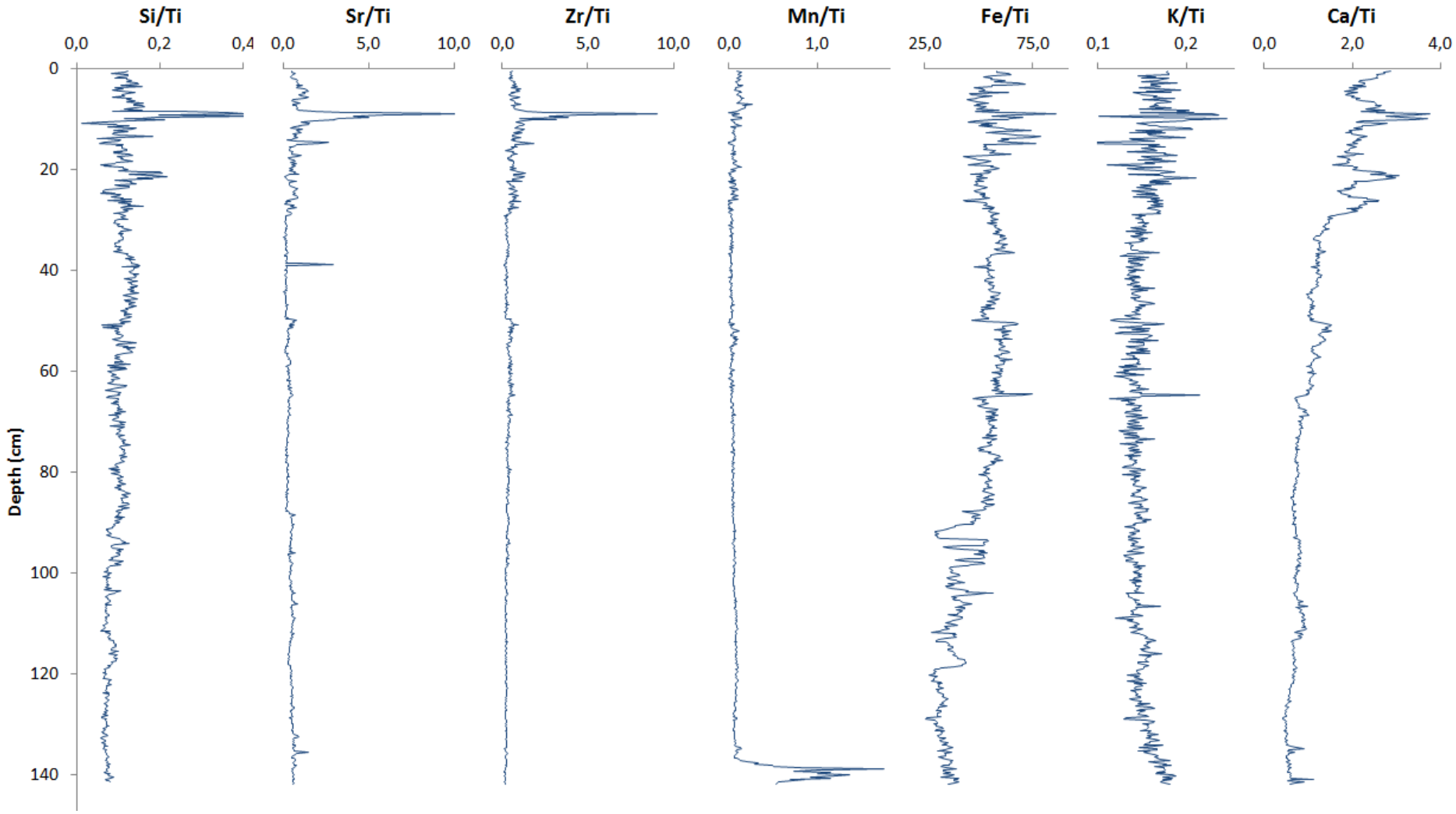

Figure 16 Ti ratios for elements Si, Sr, Zr, Mn, Fe, K and Ca for FS.

6. Discussion

Acting as the main water reserve of southern Africa (Grab, 2010), the wetlands of Lesotho are very important to study in order to understand past and recent changes. Here, the results from several exploratory organic sequences from the Sani Valley in eastern Lesotho are presented and interpreted in order to understand wetland development and evidence of climate changes during the last ca. 2 800 years. The organic-rich sediments have been analyzed for a series of chemical and physical proxies, which here will be discussed in terms of elemental variations, mineral content and organic material characterization. Furthermore a hypothesis on the development of the wetlands in Sani Valley is presented and linked to previously determined climate variations in Lesotho and southern Africa. Additionally, a chronology covering the last 2 800 years is discussed, including interpretations of the occurrence of age reversals at both sites.

The composition of an organic deposit is controlled by several external and internal factors, such as bedrock composition and catchment erosion (Kylander et al., 2011), groundwater chemistry (Charman, 2002), productivity and decomposition (Hansson et al., 2013). Many of these factors are controlled by the integrated effects of climate. The elemental and isotopic changes reflect these processes and can, in combination with other proxies, be used for interpreting changes in mineral matter input and productivity, thereby providing a means for interpretation of different wetland stages. As certain elements might play different roles at different times during wetland development (Kylander et al., 2011), it is important to investigate how the elements correlate to one another as well as to other proxies typically used in paleoclimate studies, such as bulk density and ash content.

The two wetlands sites studied here have slightly different catchments, yet they present similar stratigraphy and elemental variations throughout the sequences. In order to organize the discussion the two sequences have been divided into eight units (Table 5) based on changes in bulk density, elemental variations and C/N data. At the bottom of both sites a gravelly layer, impenetrable by the Russian corer used for sampling, was encountered at 115 cm at LB and 145 cm at FS, which means that organic matter accumulation started sometime before ca. 1 300 cal yr BP and ca. 2 800 cal yr BP at LB and FS, respectively.

Table 5 Division of the two sediment sequences into four units, based on changes in bulk density, elemental variations and C/N data. LB Units: D, C, B, A. FS Units: C, X, B, A.

	LB Units				FS Units			
	Unit D	Unit C	Unit B	Unit A	Unit C	Unit X	Unit B	Unit A
Depth (cm)	109-86	86-65	65-15	15-0	144-188	118-91	91-66	66-0
Age (cal yr BP)	>1320-900	900-800	800-50	50-0	>2825-2600	2600-2200	2200-600	600-0

6.1. Elemental variation controls

When interpreting XRF data from organic rich sediments it is important to consider dilution (closed-sum effect), which in essence means that any elemental variations might actually be a response to varying amounts of organic content within the analyzed material rather than actual concentration variations (Löwemark et al., 2011). Therefore, the data is normalized and often Ti is chosen for this task as it is abundant and does not weather (Chambers et al., 2012) or plays any important biological role (Kylander et al., 2013b). Any changes in these ratios will imply divergence from any covariance with Ti, which greatly can assist in the interpretation of the elemental data and the division of elements into groups. Here, the elemental ratios have been used to identify biological productivity (Ca/Ti, (Kylander et al., 2011)), diatom production versus detrital input (Si/Ti, (Peinerud, 2000)) and redox conditions (Fe/Ti, Mn/Ti (Muller et al., 2008)).

Out of the suite of elements analyzed, eight were chosen to represent different processes in the catchments. Here, the elements have been divided into three groups: lithogenic, redox indicators and elements involved in biological processes. This division is based on the interelemental correlation matrices of the scanning XRF data for each site (Table 2, Table 4) and for each individual unit (Appendix B – Table 6, Table 7) in combination with the Ti-ratios. Titanium correlates strongly with Si, K and Sr over both sequences, suggesting that these elements are of mainly lithogenic origin. This does however vary within the different units, as Si also correlates strongly to Ca, Fe (LB unit B, Table 6, and FS units A, B, Table 7). This would indicate relations to productivity, in the form of diatoms, further supported by coupling to other productivity proxies such as Si/Ti and C/N. Fe correlates strongly with lithogenic elements Ti, Si and K, suggesting its origin is mainly from detrital input. However, the Fe/Ti ratio tells another story and Fe seems to behave differently at different depths. This is connected to the soluble nature of Fe, which is increased in more oxic conditions (Croudance et al., 2006), why Fe here is considered to be a redox indicator. Nevertheless, it is important to keep in mind that Fe can also be immobile under anoxic conditions and mobile during oxic (Muller et al., 2008). Mn behaves

somewhat similar to Fe, apart from some sequences where Mn mirrors Fe, as well as in the bottommost 10-20 cm where concentrations are up to ten times higher than in the rest of the sequences. Mn is hence considered a redox indicator and can together with Fe be used to distinguish oxic conditions from anoxic (Muller et al., 2008). Ca has strong correlation with all other elements, but differs greatly from them when the lithogenic component is omitted in the Ca/Ti ratio. Here there is a clear decoupling from the rest of the elements towards the top of the sequences, as well as a strong relation to productivity proxies, such as C/N and Si/Ti, suggesting that it acts mainly in biological processes. However, this differs throughout the different units and will be discussed separately below.

6.2. Detrital input controls

Generally in wetland studies, increases in bulk density is seen as a sign of greater decomposition of the material (e.g. Kylander et al., 2013a), although here it appears to also be strongly influenced by detrital material brought to the wetland by surface runoff and strong winds. In order to characterize this mineral material, the aforementioned bulk density combined with ash content, could be used to estimate the mineral portion of the recovered sequences. Additionally, the occurrence of different size fractions have aided in the interpretation of the hydrological factor, in terms of estimating under what conditions the sediments have been deposited. The variations of the lithological elements, especially Ti-ratios such as Zr/Ti (grain size indicator) and Si/Ti (indicator of detrital silica or diatom productivity) have provided further insight into this matter.

It has here been assumed that the mineral matter is fluvial and aeolian in character, however some fraction of the mineral matter might have a biogenic or volcanic origin, although no effort have been made in this study to do any distinction between these. Nonetheless, the deposits are most likely mainly fluvial, where the majority of the detrital component has been transported to the site with surface runoff during wetter periods, possibly coupled with some aeolian deposition during more arid periods. However, since winds in this region can be quite strong and might be able to relocate grains of larger size fractions, such as sand (S. Grab pers. comment), comparison with other proxies is necessary to draw any conclusions on sediment deposition conditions.

In an attempt to estimate grain size, the ratio Zr/Ti has been used, as Zr is mainly associated with coarser silt to and size fractions, while Ti is associated to clay minerals (Kylander et al.,

2011). An increase in Zr/Ti would suggest increased hydrological activity in the form of more and larger grained mineral matter transported to the deposit following high precipitation periods with increases in catchment erosion and surface runoff. Zr/Ti presents little variation at both sites up to ca. 30 cm depth, although values at LB oscillates at a slightly higher relative amplitude. This suggests that small changes in grain size over the interval covered here, with some more well defined grain size increases during the last couple of hundreds of years. Possibly, this could indicate that seasonal variations have been captured, as these layers are less decomposed than those below. However, this could not be confirmed without performing any grain size analyses.

The composition of the basalts of Sani Pass have been analyzed by Ramluckan (1992) and intermediate values for the basalt groups studied is: SiO_2 (around 50%), Al_2O_3 (ca. 15%), iron oxides Fe_2O_3 and FeO (ca. 12%) and CaO (around 10%). This bedrock composition affects the groundwater, enriching it in e.g. CaO and K_2O (van Zinderen Bakker & Werger, 1974). This enrichment, especially in CaO needs to be considered when looking at the elemental data, mainly Ca/Ti, from which distinctions can be made between a lithological or biological origin. Similar caution need to be taken in considering the Fe content, as increased minerogenic content would affect the concentration.

The two mass deposition events seen both at LB (Unit C) and at FS (Unit X) are most likely to indicate periods of high precipitation. This have possibly been coupled with decreased slope vegetation, when large amounts of water have transported mineral and organic material from the catchment into the deposit. The units representing these events present increases in the majority of the element concentrations as well as on bulk density, $\delta^{13}C$ and C/N. The amount of material deposited during these rather short intervals, 9-800 cal yr BP (LB) and ca. 2600-2200 cal yr BP (FS), must have been rather substantial as these units cover ca. 20 cm at both sites. Similar events have been encountered in other studies, e.g. Berntsson et al. (2015) who presents data where Si/Ti and the sand size fraction increases significantly, while many other proxies, such as TOC remains steady.

6.3. **Organic material characterization**

Organic matter content varies from 6 to 54 %, averaging around 20% at both sites, suggesting rather high input of minerogenic content. The material in these deposits will simply be referred to as organic-rich sediments, since e.g. peat in general is classified as containing more than 65% dry weight organic matter (Charman, 2002). Carbon content, C/N and $\delta^{13}C$ have been used in an attempt to discern decomposition from productivity, and thereby also considering the input of minerogenic material into the deposit. In organic rich deposits the carbon content varies naturally with depth, as a result of carbon loss from the material in the form of methane, carbon dioxide and dissolved organic carbon (Bindler, 2006). C/N is commonly used for distinguishing between terrestrial plants and algal material (Meyers, 1994), but can also be a means to estimate decomposition degree (Bindler, 2006). Changes in $\delta^{13}C$ values can be used as an indicator of decomposition (Bindler, 2005), as well as to estimate changes in water level (Charman, 2002; Large et al., 2009), insolation (Hong et al., 2001) and the occurrence of high precipitation events (Margalef et al., 2013).

As C/N values range from ca. 14 to 33, the composition of the organic material have here been characterized as consisting of a mixture of terrestrial vascular plants and algae (Meyers, 1994). Unit D at LB differs from this classification, as it presents the highest values, suggesting mainly terrestrial plants, possibly grass or heath, both common in these areas, apart from on and near the wetlands, where herbs and sedges dominate (Grab, 2012). This would imply that the vegetation at LB in the time period covered by unit D was not a wetland environment as it is today, but possibly more similar to that on adjacent slopes. At both sites C/N values increase with age, suggesting a transition to more algae production towards present day, which would be favored by a higher water table. As for FS, C/N ratios remain more or less steady throughout the entire sequence, suggesting little variation in the vegetation composition. At some depths, however, there are decreases implying a mixture of terrestrial plants and algae. This might be an indication of that FS is an older and more evolved wetland than LB, as it does present a longer fibrous and more organic sequence, which might have been even longer if not interrupted by mass-wasting events and possible surface erosion.

$\delta^{13}C$ varies slightly, from -28.6 to -25.95‰ (LB) and -26.82 to -25.56‰ (FS), suggesting little variation in vegetation composition. Land plants with C3 metabolism are characterized by $\delta^{13}C$ values ranging from -28 to -25‰ (Meyers, 1994), why it is concluded that C3 plants has been the dominating type during the time covered here. This is in agreement with studies in Lesotho

by Parker et al. (2011) and Roberts et al. (2013), who found that the vegetation type changes with altitude and that the dominating vegetation above 2 700 m a.s.l. is C3. $\delta^{13}C$ variations in the LB sequence suggests increasing decomposition (carbon loss) upwards, while FS values fluctuates slightly around its baseline value. Changes in $\delta^{13}C$ can, as mentioned above, be the result of changes in water table level and insolation, which in turn affects the rate at which the organic matter can decompose, as well as to what extent new plant material is produced.

Variations in Ca/Ti can indicate changes in productivity, mineral matter source and/or amount of surface erosion (Kylander et al., 2013b). However, as the composition of the bedrock is the same in Sani Valley and because any fluvial input of external material would be hidden in the local signal, a change in mineral source can be excluded from this. More likely is that Ca, and Ca/Ti, reflects changes in biological activity (productivity) within these wetland areas. Also, the upmost layers at FS have a more organic and fibrous character than do those at LB, implying less decomposition and hence wetter conditions in recent times than at LB. Ash contents are similar at both sites, even though stratigraphy suggests more organic material at FS, a fact that might be explained by differences in detrital input, with higher rates at LB.

6.4. LB units

Unit D (109-86 cm)

The unit covers >1 320 (109 cm) to 900 BP (86 cm), and is defined by higher minerogenic and less organic content than the other units. General decreases can be seen in C/N ratio as well as in Fe and Ti, with a rather steep increase of carbon. Higher concentrations of Fe and Ti in combination with higher bulk density and the presence of sand and gravel suggest the material was deposited in a limnic environment, most likely a shallow pond. Detrital material input is most likely to have been transported to the deposit during periods of high precipitation, and thereby higher water energies, in order to relocate the heavier size fractions. Ash content varies little, suggesting not much difference in composition, but might also be attributed to less organic material dilution (lower carbon content). It is also quite possible that there have been deposition during "pond-conditions" varied with drier periods, enabling decomposition and resulting in less organic material left.

Unit C (86-65 cm)

Although rather long (ca. 20 cm), this unit appears to be deposited in a short period of time and dating of the transitions to adjacent units suggests this occurred around 900-800 cal yr BP. Large increases in all proxies except ash content suggests a mass wasting event with similar composition as the adjacent units. An increase in C/N suggests input of organic matter from the surroundings and while bulk density and ash content vary little, a slight increase can be seen in Fe/Ti. This in addition to the sharp lithological transition to the layer above, suggests a period of one or several events where large amounts of organic and minerogenic matter from the surrounding slopes have been deposited, ending as abruptly as it started. It is suggested that this have happened during a period of heavy precipitation and perhaps little slope vegetation, enabling more material from surface erosion to enter this deposit. In the radiograph (Figure 17) this sequence presents gradually increasing organic material towards the top of the unit, except a band of about 2-3 cm with more minerogenic material deposited at the end of this period (at ca. 70 cm).

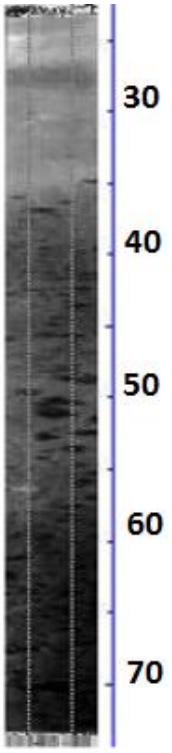

Figure 17 Radiograph of core B2-C2 from LB. Depth in cm.

Unit B (65-15 cm)

This unit is characterized by rather steady states for the majority of the proxies, e.g. C/N, Mn/Ti and Sr/Ti and covers the period from around 800 to 50 BP. Slight increases can be seen for Si/Ti, coupled with a decrease of lithogenic elements and an increase in Ca/Ti, suggesting increased biological production. Generally decreasing bulk density and ash content further supports the idea of higher productivity and/or less detrital input upwards. Stratigraphically there is little variation in this unit, although slightly more preserved plant parts were observed towards the top of the unit. This suggests steady conditions, with deposits likely to have accumulated in a wetland environment, with little variation in water and nutrient availability.

Unit A (15-0 cm)

This unit represents the active organic layer and covers recent depositions (<50 years old), something that can be seen already when examining the stratigraphy, displaying seemingly very recently buried plant material. The increase in bulk density in the top 10 cm is likely due to compaction by grazing animals, as opposed to decomposition, since this is accompanied by increases in the majority of the XRF data, as well as $\delta^{13}C$.

6.5. **FS units**

The sequence from FS was divided into four units, where three of them (A, B and C) represents different conditions and unit X seems to indicate a mass wasting event, or similar. The sequence is considered continuous down to ca. 65 cm, and thereafter discontinuous, as this site probably have been subjected to mass deposition events and surface erosion. Based on the age model there will be some approximate dates for the time periods these units cover, although these should not be considered all too reliable.

Unit C (144-118 cm)

In this unit, covering the oldest part (>2 825 to ca. 2 600 cal yr BP) of the FS sequences, the lithogenic elements Ti and Fe, as well as bulk density decreases accompanied by slight increases in Ca/Ti and C/N. Mn/Ti peaks at 138 cm and thereafter decreases 40 fold, simultaneously as a drop in C/N. At 134 cm $\delta^{13}C$, bulk density and K/Ti drops, whereas there is a peak in Ca/Ti. All this implies gradually decreasing detrital input and towards the top of the unit a slight increase in productivity. Sand and some gravel in the bottommost ca. 10 cm suggests similar deposition environment as for Unit D in LB, a shallow pond. Lowest dated sample is at 129 cm (2 740 cal yr BP), which was chosen as it was the deepest sample where plant macrofossils could be discernable.

Unit X (118-91 cm)

This unit covers around 2 600-2 200 cal yr BP and is characterized by rapid increases in Ca/Ti, C/N, bulk density, $\delta^{13}C$, Ti and Fe peaking around 113 cm (ca. 2 580 cal yr BP), only to thereafter decrease again and return to similar values as in the top of unit C. A sharp drop in Fe/Ti at 93 cm (ca. 2 300 cal yr BP) suggests temporarily more oxic conditions. This is coupled with increased bulk density, followed by sharp drops in Ti and Fe, which could be indicative of compaction following increased decomposition. However, no such changes is seen in e.g. C/N. The most likely scenario here is that it up to the transition between unit C and X was normal conditions, as nothing else indicate the opposite. Sometime after this, and before 1700 BP, heavy rainfall is likely to have caused largely increased surface runoff and erosion, adding onto the sequence with older material from the surroundings. Generally, there is high correlation between all elements, suggesting a large input of mixed detrital and organic material.

Unit B (91-66 cm)

As for unit B in LB, this unit (ca. 2200-600 cal yr BP) too is characterized by rather steady conditions and presents little variation in the majority of the proxies. There is however some oscillation for Si/Ti, Fe/Ti, as well as a slight increase in Ca/Ti as well as C/N peaks at 87 and

77 cm. This would suggest a rather stable deposition environment, likely some type of pond transitioning into more of a wetland upwards, with some diatom production and a steady relation between deposition of both organic and detrital matter.

Unit A (66-0 cm)

This unit covers ca. 600 cal yr BP until present, of which the upper ca. 15 cm likely represents the active layer, which is very fibrous and contains plenty of recently buried plant material. At the transition between unit B and A, there is an age reversal of about 300 years, which might have been caused by a high precipitation event transporting material into the deposit from the surroundings. Above this transition, there is a general trend of increasing organic material and decreasing minerogenic, as can be seen in the declining bulk density, ash content and Ti, as well as increased productivity, as indicated by a strong increase for Ca/Ti, especially from ca. 30 cm and upwards. Peaks in Si/Ti, Zr/Ti, Ca/Ti and C/N at ca. 21 suggests a temporarily high organic productivity, accompanied by the deposition of slightly finer-grained detrital material. This is followed by drops in all mentioned proxies, as well as an increase in $\delta^{13}C$, which could suggest a lowered water table (Charman, 2002), resulting in increased decomposition. This is further supported by the declining C/N ratio, which suggests carbon loss (Bindler, 2006).

6.6. Wetland development

Based on the data analyzed in this study, four distinct units have been identified at both sites: a bottommost layer representing a "pre-wetland stage", above which is found a unit representing a period of highly increased matter input, both organic and minerogenic. Next comes a longer unit, representing slightly oscillating, but steady conditions implying a continuous wetland stage and lastly an active, somewhat compressed unit at the top. However, there appears to be additional factors to consider for FS, as this sequence is not considered continuous, due to rather large age reversals of ca. 500 (between 111 and 91 cm) and 300 years (65 cm). The most likely cause for this is deposition of older catchment matter onto the younger material, as a consequence of one or several high precipitation events, possibly accompanied by surface erosion. An event of similar character seems to have taken place at LB around 900-800 cal yr BP, although age reversals here are more modest (ca. 100 years).

The units from these two sites do not correlate time wise and the accumulation of organic material appears to have commenced earlier at FS (ca. 2 800 cal yr BP) than at LB (ca. 1 300 cal yr BP). This implies that the wetlands studied here are younger than deposits in other parts of this region. Several other studies have been performed on organic deposits in southern Africa,

and many of these presents basal ages of the organic material to around 5 000 to 3 500 BP, although some are as old as 15 000 BP (Meadows, 1988). In Lesotho, however, van Zinderen Bakker & Werger (1974) reports dates of 8 020 ± 80 BP and Rosen et al. (1999) dates the organic material to 4 720 yr BP in Tiffindell, South Africa, near the border to southern Lesotho. Few studies have been performed in Sani Valley, but Marker (1994) encountered organic deposits with basal ages of around 5 000 yr BP and dates the oldest samples to 13 490 yr BP. However, she also states (Marker, 1995) that the youngest organic deposits 2 300 and 3 100 BP.

Already when looking at the stratigraphy, it is evident that these wetlands have undergone several transitions and that these stages are more or less clearly represented by the organic and minerogenic material deposited. Both sites present a bottom gravelly layer, which need not be the deepest layer of the sedimentary sequence, but instead might have been caused by high precipitation events bringing top soil into the deposits. This was also encountered by Marker (1994), who discovered two peat layers separated by a gravelly layer and also suggested heavy rains. However, if there are no more organic matter below, this gravel layer would represent the transition between mainly minerogenic deposition to a mix of both minerogenic and organic.

Whether the gravel is the bottommost layer of these deposits or not does not affect the fact that the unit above this is similar too at both sites, with high minerogenic content (clay/silt), most likely to have settled beneath a higher water table than at present. With this in mind it is likely there have been some kind of small shallow lakes or ponds in these areas at around 3 000-1 000 years BP. Eventually, these ponds are believed to have been filled in partly during runoff events and, when conditions allowed, by plants and roots. In time this have led to pond overgrowth, followed by different wetland stages during alternating wetter/drier conditions. During at least the latest 200 years, the wetlands have been subject to anthropogenic effects such as pollution and cattle grazing and trampling, likely to cause a compaction of the deposits' topmost layers (Grundling et al., 2014).

As have been mentioned earlier, the wetlands are mainly fed from beneath by groundwater (Backéus, 1989), enabling them to continue to grow even during drier times. However, it is very difficult to hypothesize on how long periods the wetlands could have manage without any precipitation refilling of the groundwater reserves. Marker (1995) concludes that present climate in Lesotho is too dry for wetlands to have permanent water access, and says the sites she studied represents former wetland conditions. This, however, is not the case at FS and LB,

as these are active wetlands. Nevertheless, the seasonal changes needs to be taken into account too, as an additional factor in the development of these wetlands. Aerial photographs of the Sani Valley are presented in Figure 18 (taken in early spring, November) and Figure 19 (taken in early summer, February). In the one taken in February, the extent of the wetland areas are clearly visible, whereas they are barely discernable in the photograph from November.

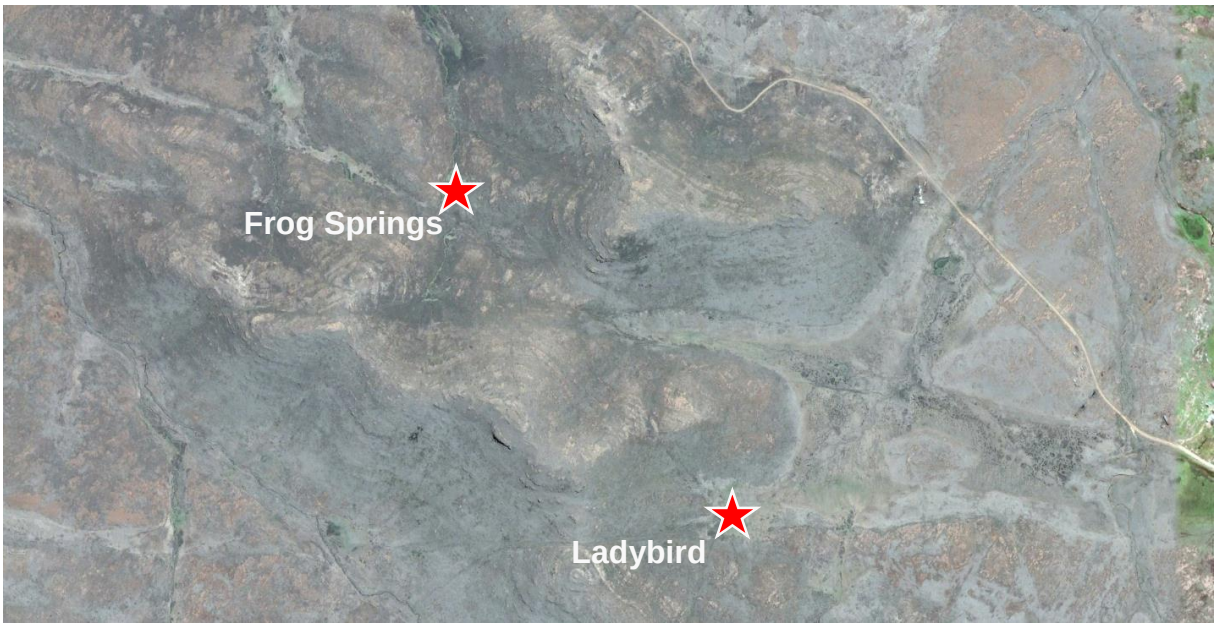

Figure 18 Aerial photograph of the Sani Valley, photo date: 2013-11-13 (early spring). Source: Google Earth.

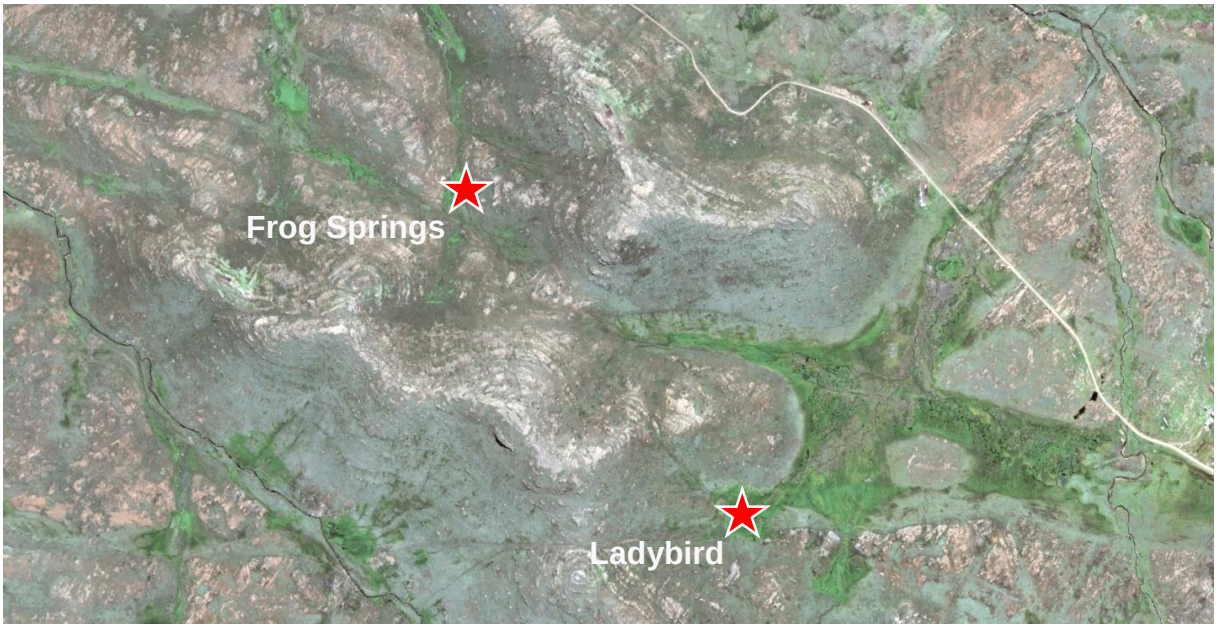

Figure 19 Aerial photograph of the Sani Valley, photo date: 2013-2-22 (late summer). Source: Google Earth.

Considering the diatoms, they too provide insight into the different wetland stages. Fitchett (2016) identified a total of 24 diatom species in the samples from FS and defined three wetland stages, similar to those identified here. Zone FSP3 is defined as rather dry and possibly with

the occurrence of small isolated, possibly seasonal, shallow ponds. Zone FSP2 is defined as containing species indicating an increasing wetland and surface water area. This coincides with the sequences containing age reversals. Zone FSP1 contains the largest diatom diversity, suggesting varying but warming climate. The appearance of certain species (e.g. *Gomphonema parvulum* and *Cymbella laevis)* are interpreted as indicators of pollution effects from human activity and occur at in the interval covering the last ca. 50 years.

In summary, the wetlands of today are thought to have developed through a series of steps, starting with the formation of alpine (turf exfoliation) pans in poorly drained areas, which are more likely to have developed during longer cold periods (Grab, 2010). Organic-rich sediment accumulation started at ca. 1 300 cal yr BP and ca. 2 800 cal yr BP at LB and FS, respectively, likely marking the transition from colder more arid to warmer more humid climate. During periods of high precipitation, both seasonal and more long termed, the pans have probably been filled up with water, creating small ponds, an environment suitable for aquatic vegetation and algae. The steady wetland conditions were initiated at FS around 2200 cal yr BP, possibly earlier, but in that case that information have been hidden by the mass wasting event in unit X. For LB, these conditions prevailed from ca. 800 cal yr BP. This implies a transition into wetter, and possibly warmer conditions, leading to increased production of organic material, eventually filling in the ponds, accompanied by mineral input from catchment runoff. There is also evidence of high detrital input events at around 2600-2200 and 900 cal yr BP, suggesting either increased precipitation or decreased slope vegetation, or both. These stages and possible environmental conditions are summarized in Figure 20.

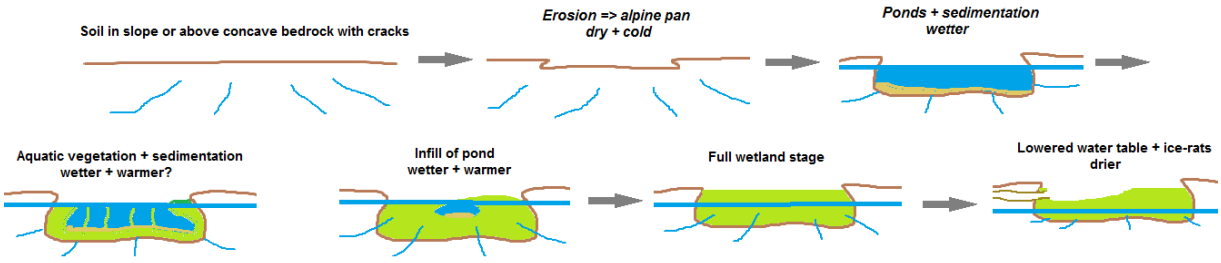

Figure 20 Schematic over wetland development stages for the two sites.

6.6.1. Chronology & age reversals

The chronology of LB is considered to be continuous throughout, as there is no evidence suggesting the opposite. At both sites, age reversals of between 500 and 100 years have been encountered, where older material have been deposited above younger. This have resulted in age reversals, which leads to a somewhat unreliable age model, especially for FS, as this occurs twice. Other studies in the area have had similar problems, e.g. Marker (1994) who encountered

both age reversals and interbedded gravel layers. As was discussed by Backéus & Grab (1995), heavy rains cause large amounts of muddy water to flood the wetlands, which might be the reason for date reversals and other issues that have appeared when analyzing samples from these sites. They also mention that these severe rainfalls might even cut gullies into the wetland itself, a fact that could affect the hydrology within the wetland. Additionally, the top layers might also be affected by the burrowing of rodents during drier times, especially that of ice rats (*Otymos sloggetti robertsi*), which live close to the wetland edges (Grab, 2012).

The effects of frost action is also important to take into account in interpreting these results. As have been discussed in several studies (e.g. Grab, 2002; Boelhouwers & Meiklejohn, 2002), frost occurs from May to August and can have severe impact on the top layers of the soil and hence the top layers of the wetland sites studied here. Age reversals could also be due to frozen organic material moving as blocks within the deposit or infilling of old carbon through cracks, if dry and cold enough for the top soil layers to freeze (Bindler et al., 2005).

One specific reason for the age reversals cannot be determined, as there are many different factors affecting it in this case. Most probable reasons are high precipitation events bringing organic material to or from the wetland, frost heaving, burrowing by ice rats and/or trampling/grazing by cattle. Impacts from cattle is not likely to be the cause of the oldest age reversals, as herders and livestock did not arrive to the Sani Valley until late 19th century (Grab, 2010). Yet another reason for the reversed dates could be root contamination, however this is less probable as great attention was given during picking of the macrofossils to minimize this effect.

6.7. Comparison with other studies and future research

Studies made in southern Africa on temperature and precipitation during the late Holocene (ca. last 5 000 years) show that changes to colder climate occur mainly during three periods: at 4 500-4 000 BP, 3 000-2 000 BP and over the last 1 000 years, where temperature decreases of 1-2 ºC have been suggested (Jerardino, 1995). Furthermore, Marker (1994) states that the period from 2 000 to 1 000 BP may have been wetter, transitioning into drier conditions over the last 1 000 years. These variations have also been recorded in the oxygen isotopes derived from speleothems at Cango Caves (South Africa), where several cool events were identified between 3 100 and 2 500 BP, a shorter event at 1 300 BP and a longer lasting cold period at 400-200 BP (Talma & Vogel, 1992). Other studies have presented increasingly wetter conditions after 2 000

cal yr BP and a humid period around 2 200-890 cal yr BP (Norström et al., 2014). Some of these established changes in southern African climate can be linked to the changes identified from the material studied here, e.g. the steady wetland stages from around 2 200 cal yr BP in FS, which coincides with the wetter period identified by Marker (1994) or the transition from mainly minerogenic to more organic accumulation at 1 300 and 2 800 cal yr BP, which occurs in between the cold periods defined by Jerardino (1995). However, shorter global events that have been identified in other studies (e.g. Chase & Meadows; Chase et al., 2015), such as the medieval Warm Epoch (900-1 300 AD) and the Little Ice Age (1300-1 850 AD) are not possible to discern here, especially since there is no co-occurrence of any of the wetland stages identified between the sites of the Sani Valley. Additionally, more dating is needed in order to provide a more reliable age model.

Studies on past climate in Lesotho are few and is less investigated than the climate of the rest of southern Africa. Out of the existing studies, many are based on archaeological finds rather than botanical or sedimentary evidence (Parker et al., 2011). This in addition to the fact that the wetlands of Lesotho are important water reserves for the drier parts of southern Africa (Grab, 2010), increases the need for better understanding of the wetlands and their history. Further paleoclimatological research in this area is needed, both based on material from previously sampled sites as well as new ones. One conclusion from this project has been that the choice of sample location is of utmost importance, as the harsh climate of highland Lesotho can affect even the most sheltered wetland. One suggestion would be to sample wetlands at higher altitudes, with fewer surrounding hillslopes, where surface runoff would be less.

7. Conclusions

Based on the chemical and physical proxies used in this study, characterizations have been made for the mineral matter, the organic material as well as what roles the different elements play. The two recovered sequences have been divided into four units each, corresponding to different stages in the development of the present day wetlands. Dating of first occurrences of organic material have led to the conclusion that organic accumulation have commenced sometime before 1 300 (LB) and 2 800 cal yr BP (FS). Both sites have thereafter undergone several stages of different character, including several occurrences of mass wasting events, bringing in older material onto the older deposits and likely being the reasons of the encountered age reversals. The majority of the mineral matter is thought to have been transported to the deposit mainly by surface runoff, but also by the strong winds common to the area. However, no attempt to discern these from other possible sources, such as biogenic or volcanic, were made in this study. Considering the vegetation, it has here been characterized as C3 metabolizing plants, which is in accordance with other studies as well. Some similarities can be seen with other sites in the area and in other parts of southern Africa, although coupling in time are difficult to discern due to few dated samples. Future research of similar character is suggested, so as to get a better understanding of how the wetlands of Lesotho function today and how they have evolved throughout history.

8. Acknowledgements

First and foremost I would like to give a very big thanks to my supervisor Malin Kylander, who has been of great support during this project, even during the *slightly* stressful last weeks. I am very grateful for having had the opportunity to work with you and with these samples. And how will I ever be able to forget our very eventful (cold) trip to South Africa and Lesotho?

Jenny Sjöström is thanked for showing me (and the rest of the group at Sani) how to work a Russian corer, for teaching me about diatom preparation and for her support during the extent of this thesis. Great thanks goes to Elin Norström for instructing me in how to prepare and mount diatom samples, and to Carina Johansson for all her help in the lab, with everything from finding lab equipment to interesting discussions. Heike Siegmund is thanked for her excellent instructions and for performing the C/N analyses. Richard Bindler and Johan Rydberg at Umeå University are thanked for taking good care of me during my visit with them and for performing the XRF analyses. Stefan Grab from the University of the Witwatersrand, Johannesburg, is thanked for being an excellent guide and host for us during the time in Lesotho and South Africa, and for interesting conversations and fun field work. A great thank you also goes to Jennifer Fitchett for taking time to analyze the diatoms.

I would also like to thank my friends and family for their great support during times when it felt like there would never come anything of this project. A special shout-out goes to fellow Master student and desk neighbor Max Holmström, for your ability to take my mind off the stress once in a while. Finally, thank you to everybody else at IGV for a year filled with many laughs, inspiring conversations and lots of great memories.

References

Ashley, G.M., Goman, M., Hover, V.C., Owen, R.B., Renaut, R.W. & Muthama Muasya, A., 2002. *Artesian blister wetlands, a perennial water resource in the semi-arid rift valley of East Africa.* Wetlands 22 (4), 686-695.

Backéus, I., 1989. *Flarks in the Maloti, Lesotho*. Geografiska Annaler 71 A (1-2), 105-111.

Backéus, I. & Grab, S., 1995. *Mires in Lesotho*. Gunneria 70, 243-250.

Battarbee, R.W., Jones, V.J., Flower, R.J., Cameron, N.G., Bennion, H., Carvalho, L. & Juggins, S., 2001. *8. Diatoms*. In: Smol, J.P., Birks, H.J.B. & Last W.M. (eds.), 2001. Tracking Environmental Change Using Lake Sediments. Volume 3: Terrestrial, Algal, and Siliceous Indicators. Kluwer Academic Publishers, Dordrecht, The Netherlands.

Bindler, R., Martínez Cortizas, A. & Blaauw, M., 2005. *Comment on "Atmospheric Mercury Accumulation Rates between 5900 and 800 Calibrated Years BP in the High Arctic of Canada Recorded by Peat Hummocks".* Environmental Science & Technology 39 (3), 908-909.

Bindler, R., 2006. *Mired in the past – looking to the future: Geochemistry of peat and the analysis of past environmental changes.* Global and Planetary Change 53, 209-221.

Blauuw, M., 2010. *Methods and code for 'classical' age-modelling of radiocarbon sequences*. Quaternary Geochronology 5, 512-518.

Boelhouwers, J.C. & Meiklejohn, K.I., 2002. *Quaternary periglacial and glacial geomorphology of southern Africa: review and synthesis*. South African Journal of Science 98, 47-55.

Chambers, F.M., Beilman, D.W. & Yu, Z., 2010. *Methods for determining peat humification and quantifying peat bulk density, organic matter and carbon content for palaeostudies of climate and peatland carbon dynamics.* Mires and Peat 7, 1-10.

Chambers, F.M., Booth, R.K., De Vleeschouwer, F., Lamentowicz, M., Le Roux, G., Mauquoy, D., Nichols, J.E. & van Geel, B., 2012. *Development and refinement of proxy-climate indicators from peats.* Quaternary International 268, 21-33.

Charman, D., 2002. *Peatlands and environmental change*. Wiley, West Sussex, England.

Chase, B.M. & Meadows, M.E., 2007. *Late Quaternary dynamics of southern Africa's winter rainfall zone*. Earth-Science Reviews 84, 103-138.

Chase, B.M., Lim, S., Chevalier, M., Book, A., Carr, A.S., Meadows, M.E. & Reimer, P.J., 2015. *Influence of tropical easterlies in southern Africa's winter rainfall zone during the Holocene.* Quaternary Science Reviews 107, 138-148.

Cohen, A.S., 2003. *Paleolimnology: The History and Evolution of Lake Systems*. Oxford University Press: Oxford.

Croudance, I.W., Rindby, A. & Rothwell, R.G., 2006. *ITRAX: description and evaluation of a new multi-function X-ray core scanner.* In: Rothwell, R.G., 2006. New Techniques in Sediment Core Analysis. Geological Society, London, Special Publications, 267, 51-63.

Dobrowolski, R., Pidek, I.A., Alexandrowicz, W.P., Halas, S., Pazdur, A., Piotrowska, N., Buczek, A., Urban, D. & Melke, J., 2012. *Interdisciplinary studies of spring mire deposits from Radzików (south Podlasie lowland, east Poland) and their significance for palaeoenvironmental reconstructions*. Geochronometria 39 (1), 10-29.

Dypvik, H. & Harris, N.B., 2001. *Geochemical facies analysis of fine-grained siliclastics using Th/U, Zr/Rb and (Zr+Rb)/Sr ratios*. Chemical Geology 181, 131-146.

Fitchett, J., 2016. *Frog springs diatom report (un-published).* University of the Witwatersrand, Johannesburg, South Africa.

Grab, S., 1997. *Thermal Regime for a Thufa Apex and its Adjoining Depression,Mashai Valley, Lesotho*. Permafrost and Periglacial Processes 8 (4), 437-445.

Grab, S., 2002. *Turf exfoliation in the high Drakensberg, southern Africa*. Geografiska annaler 84 A (1): 39-50.

Grab, S., 2010. *Alpine turf exfoliation pans in Lesotho, southern Africa: Climate-process-morpholocigal linkages*. Geomorphology 114, 261-275.

Grab, S., 2012. *On the burrowing impacts of ice rats Otomys sloggetti robertsi at a wetland fringe in the Afro-alpine zone, Lesotho*. South African Geographical Journal 94 (1), 75-84.

Grundling, P-L., Linström, A., Fokkema, W. & Grootjans, A.P., 2014. *Mires in the Maluti Mountains of Lesotho*. Mires and Peat 15 (9), 1-11.

Hansson, S.V., Rydberg, J., Kylander, M., Gallagher, K. & Bindler, R., 2013. *Evaluating paleoproxies for peat decomposition and their relationship to peat geochemistry*. The Holocene 23 (12), 1666-1671.

Hogg, A.G., Hua, Q., Blackwell, P.G., Niu, M., Buck, C.E., Guilderson, T.P., Heaton, T.J., Palmer, J.G., Reimer, P.J., Reimer, R.W., Turney, C.S.M. & Zimmerman, S.R.H., 2013. *SHCal13 Southern Hemisphere calibration, 0-50,000 years cal BP*. Radiocarbon 55 (4), 1889-1903.

Hong, Y.T., Wang, Z.G., Jiang, H.B., Lin, Q.H., Hong, B., Zhu, Y.X., Wang, Y., Xu, L.S., Leng, X.T & Li, H.D. (2001). *A 6000-year record of changes in drought and precipitation in northeastern China based on a δ13C time series from peat cellulose*. Earth and Planetary Science Letters 185, 111-119.

Jerardino, A., 1995. *Late Holocene Neoglacial episodes in southern South America and southern Africa: a comparison*. The Holocene 5 (3), 361-368.

Knight, J. & Grab, S., 2015. *6. The Drakensberg Escarpment: Mountain processes at the edge*. In: Grab, S. & Knight, J. (eds.), 2015. Landscapes and landforms of South Africa, World Geomorphological Landscapes. Springer International Publishing, Switzerland.

Kylander, M.E., Muller, J., Wüst, R.A.J., Gallagher, K., Garcia-Sanchez, R., Coles, B.J. & Weiss, D.J., 2007. *Rare earth element and Pb isotope variations in a 52 kyr peat core from Lynch's Crater (NE Queensland, Australia): Proxy development and application to paleoclimate in the Southern Hemisphere.* Geochimica et Cosmochimica Acta 71, 942-960.

Kylander, M.E., Ampel, L., Wohlfarth, B. & Veres, D., 2011. *High-resolution X-ray fluorescence core scanning analysis of Les Echets (France) sedimentary sequence: new insights from chemical proxies.* Journal of Quaternary Science 26 (1), 109-117.

Kylander, M.E., Bindler, R., Martínez Cortizas, A., Gallagher, K., Mörth, C-M. & Rauch, S., 2013a. *A novel geochemical approach to paleorecords of dust deposition and effective humidity: 8500 years of peat accumulation at Store Mosse (the "Great Bog"), Sweden.* Quaternary Science Reviews 69, 69-82.

Kylander, M.E., Klaminder, J., Wohlfarth, B. & Löwemark, L., 2013b. *Geochemical responses to paleoclimatic changes in southern Sweden since the late glacial: the Hässeldala Port lake sediment record*. Journal of Paleolimnology 50, 57-70.

Large, D.J., Spiro, B., Ferrat, M., Shopland, M., Kylander, M., Gallagher, K., Li, X., Shen, C., Possnert, G., Zhang, G., Darling, W.G. & Weiss, D., 2009. *The influence of climate, hydrology and permafrost on Holocene peat accumulation at 3500 m on the eastern Qinghai-Tibetan Plateau.* Quaternary Science Reviews 28, 3303-3314.

Ljung, K., Holmgren, S., Kylander, M., Sjolte, J., Van der Putten, N., Kageyama, M., Porter, C.T. & Björck, S., 2015. *The last termination in the central South Atlantic*. Quaternary Science Reviews 123, 193-214.

Lowry, C.S., Fratta, D. & Anderson, M.P., 2009. *Ground penetrating radar and spring formation in a groundwater dominated peatland.* Journal of Hydrology 373, 68-79.

Löwemark, L., Chen, H-F., Yand, T-N., Kylander, M., Yu, E-F., Hsu, Y-W., Lee, T-Q., Song, S-R. & Jarvis, S., 2011. *Normalizing XRF-scanner data: A cautionary note on the interpretation of high-resolution records from organic-rich lakes*. Journal of Asian Earth Sciences 40, 1250-1256.

Macphail, M.K, Pemberton, M. & Jacobson, G., 1999. *Peat mounds of southwest Tasmania: possible origins.* Australian Journal of Earth Sciences 46, 667-677.

Margalef, O., Cañellas-Boltá, N., Pla-Rabes, S., Giralt, S., Pueyo, J.J., Joosten, H., Rull, V., Buchaca, T., Hernández, A., Valero-Garcés, B.L., Moreno, A. & Sáez, A., 2013. *A 70,000 year multiproxy record of climatic and environmental change from Rano Aroi peatland (Easter Island).* Global and Planetary Change 108, 72-84.

Marker, M.E., 1994. *Sedimentary sequences at Sani Top, Lesotho highlands, southern Africa*. The Holocene 4 (4), 406-412.

Marker, M.E., 1995. *Late Quaternary environmental implications from sedimentary sequences at two high altitude Lesotho sites*. South African Journal of Science 91 (6), 294-299.

Mazurek, M., Dobrowolski, R. & Osadowski, Z., 2014. *Geochemistry of deposits from spring-fed fens in West Pomerania (Poland) and its significance for palaeoenvironmental reconstruction*. Quaternary Geomorphology 4, 323-342.

McCarthy, T.S., Ellery, W.N., Backwell, L., Marren, P., de Klerk, B., Tooth, S., Brandt, D. & Woodborne, S., 2010. *The character, origin and palaeoenvironmental significance of the Wonderkrater spring mound, South Africa*. Journal of African Earth Sciences 58, 115-126.

Meadows, M.E., 1988. *Late Quaternary peat accumulation in southern Africa*. Catena 15, 459-472.

Mills, S., Grab, S.W., Rea, B.R, Carr, S.J. & Farrow, A., 2012. *Shifting westerlies and precipitation patterns during the Late Pleistocene in southern Africa determined using glacier reconstruction and mass balance modeling.* Quaternary Science Reviews 55, 145-159.

Mitchell, A.A. & Ramluckan, V.R., 1996. *The basalt stratigraphy of the Sani Pass, KwaZulu/Natal Drakensberg*. South African Journal of Geology 99 (3), 251-263.

Muller, J., Kylander, M., Martinez-Cortizas, A., Wüst, R.A.J., Weiss, D., Blake, K., Coles, B. & Garcia-Sanchez, R., 2008. *The use of principle component analyses in characterising trance and elemental distribution in a 55 kyr peat deposit in tropical Australia: Implications to paleoclimate.* Geochimica et Cosmochimica Acta 72, 449-463.

Nel, W. & Sumner, P., 2008. *Rainfall and temperature attributes on the Lesotho-Drakensberg escarpment edge, southern Africa.* Geografiska Annaler 90 A (1), 97-108.

Norström, E., Neumann, F.H., Scott, L., Smittenberg, R.H., Holmstrand, H., Lundqvist, S., Snowball, I., Sundqvist, H.S., Risberg, J. & Bamford, M., 2014. *Late Quaternary vegetation dynamics and hydro-climate in the Drakensberg, South Africa.* Quaternary Science Reviews 105, 48-65.

Olaleye, A.O., Nkheloane, T., Mating, R., Mahlako, K., Rathebe, K., Letsika, F. & Rasekoele, M.G., 2014. *Wetlands in Khalong-la-Lithunya catchment in Lesotho: Soil organic carbon contents, vegetation isotopic signatures and hydrochemistry*. Catena 115, 71-78.

Parker, A.G., Lee-Thorp, J. & Mitchell, P.J., 2011. *Late Holocene Neoglacial conditions from the Lesotho highlands, southern Africa: phytolith and stable carbon isotope evidence from the archaeological site of Likoaeng*. Proceedings of the Geologists' Association 122, 201-211.

Peinerud, E.K., 2000. *Interpretation of Si concentrations in lake sediments: three case studies.* Environmental Geology 40 (1-2), 64-72.

Ramluckan, V.R., 1992. *The petrology and geochemistry of the Karoo sequence basaltic rocks in the Natal Drakensberg at Sani Pass.* MSc Thesis, University of Durban-Westville, South Africa.

Roberts, P, Lee-Thorp, J.A., Mitchell, P.J. & Arthur, C., 2013. *Stable carbon isotopic evidence for climate change across the late Pleistocene to early Holocene from Lesotho, southern Africa.* Journal of Quaternary Science 28(4), 360-369.

Rosen, D.Z., Lewis, C.A. & Illgner, P.M., 1999. *Palaeoclimatic and archaeological implications of organic-rich sediments at Tiffindell Ski Resort, near Rhodes, Eastern Cape Province, South Africa*. Transactions of the Royal Society of South Africa 54(2), 311-321.

Sene, K.J., Jones, D.A., Meigh, J.R. & Farquharson, F.A.K., 1998. *Rainfall and flow variations in the Lesotho Highlands.* International Journal of Climatology 18, 329-345.

Sliva, J. & Grundling, P-L., 2002. *Identification and Mapping of Peatlands in South Africa (IMPESA): Evaluation of resources*. IMPESA, Pretoria and Freising, 440 pp.

van Zinderen Bakker, E.M. & Werger, M.J.A., 1974. *Environment, vegetation and phytogeography of the high-altitude bogs of Lesotho*. Vegetatio 29 (1), 37-49.

Weiss, D., Shotyk, W., Rieley, J., Page, S., Gloor, M., Reese, S. & Marinez-Cortizas, A., 2002. *The geochemistry of major and selected trace elements in a forested peat bog, Kalimantan, SE Asia, and its implications for past atmospheric dust deposition*. Geochimica et Cosmochimica Acta 66 (13), 2307-2323.

Appendix A – Method descriptions

Calculating sample areas in Inkscape

- Samples were placed on a watch glass with a diameter of 10 cm and photographed with a digital camera at approximately equal distance under bright lights, minimizing shadows.
- The jpg files were imported to Inkscape v. 0.91 and resized so 10 cm in the image corresponded to 10 cm in the software.
- Filters>Color>Lightness-Contrast to change contrast to 100
- Path>Trace Bitmap
- Path>Trace Pixel Art, making sure "Convert to B-spline curves" is checked.
- To calculate the area, Extensions>Visualize Path>Measure Path. Choose "Area" and "cm" in the drop down menus, and "Fixed Angle" for Text Orientation, then press Apply. This will give the area of the sample in cm^2.

Enrichment and mounting of diatoms

Below follows a detailed preparation schedule for enriching and mounting diatoms on glass slides, adapted from Battarbee et al. (2001).

Enrichment

- Weigh 0.5-2 g of the sample in a beaker (100 mL).
- To test if the sample contains lime you can drip a few drops of hydrochloric acid 10 % (HCl). If there is a reaction (there will be bubbles), add more HCl until all lime is dissolved. Place a watch glass on the beaker.
- Mix half hydrogen peroxide (H_2O_2) and half distilled water (Milli-Q) in a spray bottle, the final concentration will be around 15-17% depending on the concentration of the hydrogen peroxide.
- Add about 20-30 mL of the diluted H_2O_2 to the beaker with your sample, place a watch glass on it and leave it in room temperature overnight. If the sample is treated with HCl, you can use hydrogen peroxide 30-35%.
- Heat the samples gradually on a water bath, preferably one with a lid and removable rings where the beakers can be placed. Set the temperature at 50 degrees C and raise it by 10 degrees every 30 minutes until you reach 100 degrees.
- Let the samples boil until there is an apparent layering between the remaining non-organic material and the upper phase, which should be completely clear. Please note that this step might take several days, do not forget to turn off the water bath during the night!
- Adding of more H_2O_2 might be needed during this step, to get the reaction going again and to avoid dry boil.
- If the reaction is violent, you can add some distilled water, or remove the beaker from the water bath and place it in cold water, to slow down the reaction.
- When the samples are done, add distilled water up to the 100 mL mark and let it settle for at least 2 hours. Decant carefully until at least 1 cm of sample suspension is left in

the beaker. Shake the beaker carefully to blend the suspension, and add distilled water to the 100 mL mark. Repeat this with 2-hour intervals until the water is clear.

- If the sample contains large particles, such as sand and gravel, shake the beaker and let it settle for 5 seconds, after which you decant the sample into a new beaker.
- Add weak ammonia solution (5 mL NH_3 to 1 L distilled water) and let it settle for 2 hours. Decant in the same manner as before until the upper phase is clear.
- Transfer the samples to test tubes with lids and let settle for 2 hours, decant one last time.

Preparing microscope slides

- Take a few drops of water with about 1 % dish soap and spread it evenly on the cover glass. Add the sample with a glass rod and spread it evenly over the cover glass. Let it dry.
- Take a small drop of Naphrax on a slide and heat it quickly on the hot plate (about 200 °C) until it is boiling. Place the cover glass with the material down on the drop of Naphrax and press gently with for example a glass rod until any air bubbles have disappeared.
- Let it dry and remove any excess Naphrax with a scalpel.

Appendix B – XRF correlation matrices

Interelemental correlation matrices

Table 6 Correlation matrices of the ITRAX data for the LB sequence by lithostratigraphic unit.

Unit		Si	K	Ca	Ti	Mn	Fe	Sr
A	K	0,09						
	Ca	0,06	0,85*					
	Ti	0,02	0,88*	0,82*				
	Mn	0,06	0,80*	0,77	0,95*			
	Fe	0,10	0,71	0,61	0,87*	0,91*		
	Sr	-0,19	0,37	0,08	0,44	0,38	0,44	
	Zr	-0,36	0,41	0,39	0,61	0,52	0,45	0,44
B	K	0,96*						
	Ca	0,91*	0,93*					
	Ti	0,95*	0,97*	0,88*				
	Mn	0,24	0,29	0,39	0,21			
	Fe	0,80	0,82*	0,85*	0,79	0,53		
	Sr	0,63	0,66	0,47	0,74	0,03	0,45	
	Zr	0,62	0,65	0,53	0,72	0,00	0,43	0,67
C	K	0,73						
	Ca	0,72	0,93*					
	Ti	0,61	0,94*	0,91*				
	Mn	0,34	0,58	0,72	0,61			
	Fe	0,58	0,90*	0,87*	0,94*	0,59		
	Sr	0,42	0,78	0,74	0,86*	0,63	0,82*	
	Zr	0,05	0,13	0,10	0,15	0,07	0,11	0,17
D	K	0,60						
	Ca	0,59	0,75					
	Ti	0,87*	0,72	0,64				
	Mn	0,29	0,59	0,78	0,33			
	Fe	0,14	0,57	0,53	0,39	0,38		
	Sr	-0,20	0,24	0,27	-0,10	0,25	0,42	
	Zr	0,28	0,00	-0,14	0,22	-0,13	-0,31	-0,38

Table 7 Correlation matrices of the ITRAX data for the FS sequence by lithostratigraphic unit.

Unit		Si	K	Ca	Ti	Mn	Fe	Sr
A	K	0,94*						
	Ca	0,79	0,82					
	Ti	0,94*	0,98*	0,78				
	Mn	0,22	0,25	0,40	0,21			
	Fe	0,92*	0,97*	0,75	0,99*	0,19		
	Sr	-0,01	-0,04	-0,04	-0,05	0,10	-0,08	
	Zr	0,02	0,06	-0,01	0,08	0,06	0,09	-0,04
B	K	0,87*						
	Ca	0,72	0,89*					
	Ti	0,87*	0,98*	0,92*				
	Mn	0,69	0,79	0,84*	0,83*			
	Fe	0,92*	0,85*	0,69	0,85*	0,66		
	Sr	0,47	0,71	0,77	0,74	0,69	0,42	
	Zr	0,45	0,64	0,66	0,66	0,57	0,44	0,75
X	K	0,91*						
	Ca	0,71	0,88*					
	Ti	0,87*	0,98*	0,92*				
	Mn	0,83*	0,89*	0,86*	0,89*			
	Fe	0,77	0,85*	0,86*	0,87*	0,83*		
	Sr	0,60	0,76	0,90*	0,83*	0,74	0,80*	
	Zr	0,73	0,76	0,70*	0,77	0,70	0,59	0,68
C	K	0,89*						
	Ca	0,65	0,61					
	Ti	0,89*	0,91*	0,54				
	Mn	0,68	0,73	0,59	0,59			
	Fe	0,87*	0,93*	0,67	0,85*	0,77		
	Sr	0,50	0,67	0,35	0,54	0,45	0,64	
	Zr	0,06	0,12	-0,29	0,18	-0,16	0,03	0,18

XRF correlations

The results from the two XRF methods were compared and are presented in Table 8 and have a strong fit, except for Si and Zr at LB and Ca at FS. Elements showing little or no variation, either due to low concentration levels (below detection limits of the instruments) or that were very noisy are excluded here (V, Ar, P, S, etc.). With the large amount of data points, all correlation is relevant but in order to make any distinctions, correlation is considered strong if values are $\geq \pm 0{,}7$ (Kylander et al., 2011). But, as the results are similar in general, the more high resolution scanning XRF data has been chosen to represent the chemical composition and has been used to construct all plots and correlation matrices.

Table 8 R^2 values for comparison of fit between WD-XRF and scanning XRF data, where higher values indicate better fit. Strongest fit can be seen between the two XRF methods for K, Ti and Mn at both sites, while weakest fit can be seen in Si and Zr at LB.

	Si	K	Ca	Ti	Mn	Fe	Sr	Zr
LB	0.10	0.78	0.47	0.82	0.44	0.85	0.56	0.24
FS	0.51	0.89	0.36	0.87	0.87	0.79	0.95	0.73